
Reply to the Interactive comments by Alan. K. Betts on 2 August, 2016

This is an interesting discussion of two IOPs during Go-Amazon, one in the wet season and the other the dry season; with three cases studies from the wet season of local, coastal and basin scale convection. It is suitable for publication with a little revision. It is written for a 'club' and needs clarity for less specialized readers.

You mention 2014-2015, but the only data you show is from 2014.
Reply: The GoAmazon2014/5 campaign is a 2-year experiment but the two IOPs that we studied were both conducted in the year 2014. This has been clarified in the revised text (lines 20-21).

Figure 1 has a 'potential site'? L93 - see below.
Reply: We have removed the unnecessary sites in the revised Figure1.

P10. Although equations (1) and (2) are based on historic literature, the units are not well defined here, and Q1, Q2 do not actually have the units of K/hr as in Figure 8. Nor does QR in (1).
Reply: Revised the equations (1), (2) and (3) as below to make the units consistent:

$$Q_1 = \frac{1}{C_p}\left(\frac{\partial \bar{s}}{\partial t} + \bar{\vec{V}}\cdot\nabla\bar{s} + \bar{\omega}\frac{\partial \bar{s}}{\partial p}\right) = \frac{1}{C_p}\left(Q_{rad} + L_v(c-e) - \frac{\partial \overline{\omega' s'}}{\partial p}\right) \quad (1)$$

$$Q_2 = -\frac{L_v}{C_p}\left(\frac{\partial \bar{q}}{\partial t} + \bar{\vec{V}}\cdot\nabla\bar{q} + \bar{\omega}\frac{\partial \bar{q}}{\partial p}\right) = \frac{L_v}{C_p}\left(c - e + \frac{\partial \overline{\omega' q'}}{\partial p}\right) \quad (2)$$

$$Q_1 - Q_2 - Q_{rad} = -\frac{1}{C_p}\frac{\partial \overline{\omega' h'}}{\partial p} \quad (3)$$

I did not find the Q1-Q2 discussion very satisfactory for Figure 8. Do you have an estimate for QR? I thought you had at least surface and TOA? Why did you not show Q1-Q2 for the case studies where the terms are larger, and different from Fig 8? Typically Q1-Q2-QR has been interpreted as the upward transport of moist static energy, h, by moist convection, but you do not discuss this, nor the added complexity of convection within the diurnal cycle.
Reply: As suggested, we revised Figure 8 by including Q_{rad} and add relevant discussion there (line 299-307). In the paper, Q_{rad} is estimated from using the radiative transfer model in the single-column model of CAM5 (Neale et al., 2012) driven by the large-scale forcing data derived from this study due to the lack of observations of Q_{rad}.

L314 time-lag… The vertically pointing cloud data are 'point' measurement (L148)? What is the effective spatial resolution of the omega field? Your discussion (L93 on) of spatial field analysis is vague, and gives no sense of the effective spatial and temporal resolution; and how the fields were effectively smoothed to get omega and other terms.

Reply: This has been clarified in lines 136-142 and 161. The cloud data are "point" measurements while the omega field (and other large-scale fields) represents an average over the analysis domain, which is ~110km in radius. The cloud data are measured at 67.8 km downwind of the center and ~170 km downwind of the east edge of the domain. Therefore, it can only see a convective system after the system propagates into the domain and is captured by the field of the view of the radar.

Reply to the Interactive comments by Enio Souza on 26 August, 2016

The authors study the behavior of some convective fields during the GoAmazon experiment, focusing on the contrast between a rainy period and a dry period. Besides, a discussion on the diurnal cycle for some cases is presented. The article worth publication after some revisions.

In line 95, the authors mention the ECMWF analysis but no word about the horizontal resolution. If the resolution is good enough, kinectic energy plays a non-neglectable role in the energy equation, and Q1 should be expressed in terms of potential temperature instead of static energy (see formulation in Yanai and Tomita, 1998, J. of Climate, p. 463).

Reply: The ECMWF analysis we got is in 0.5° resolution but the energy budget we calculate is averaging over the GOAmazon domain which is ~110km in radius (added in line 112-113). Giving that resolution, we believe that kinetic energy is neglectable in the energy equation and dry static energy is a good estimation to be used.

Another important point is the radiative heating Qrad. In studies with less time resolution, an average value can be used. One can also argue that Qrad is small compared to Q1 and Q2. However, since this study addresses both the diurnal cycle and the vertical structure of the convective heating, and Qrad do undergoes a strong diurnal cycle and presents a vertical structure that impacts on the intensity of convection, the diurnal cycle of Qrad should be properly taken into account. That variable can be easily obtained from any numerical model.

Reply: Thanks for the suggestion. Following your suggestion, we have now estimated Q_{rad} and accounted for it in the discussion of the diurnal cycle (line 271-277 and lines 299-307). In the revised paper, Q_{rad} is estimated from using the radiative transfer model in the single-column model of CAM5 (Neale et al., 2012) driven by the large-scale forcing data derived from this study due to the lack of observations of Q_{rad}.

The authors use domain-mean precipitation instead of point precipitation. In my opinion that is an outstanding advance of this study, since it provides a good framework to comparison with numerical model results for the region. Returning to the discussion of the previous paragraph, the vertical integral of Q1-Qrad, divided by the latent heat of evaporation, gives an estimative of the precipitation rate (see Eqn. 12a, by Yanai et al., 1973). This information could be easily obtained, and a comparison with the observed precipitation rate (investigating both the intensity and the correlation) could be performed.

Reply: Thank you for your comment. Because the thermodynamic equation and water vapor conservation equation are explicitly satisfied in the variational analysis and the observed precipitation is used as the constraint, the vertical integral of Q1-Qrad and vertical integral of Q2 are consistent with the observed precipitation rate implicitly. We have added a sentence to make this clear (lines 217-220).

In line 215, the authors point latent cooling due to ice melting as responsible for the minimum of Q1 observed around 600 hPa. What do the authors have to say about cumulus congestus whose top are around that level? That is a region of re-evaporation of water droplets and strong radiative flux divergence.

Reply: Thanks. We agree that besides ice melting, there could be other reasons that cause the minimum of Q1 (or the double peak structure), such as the combining effect of lower level shallow cumulus and upper level deep convection or MCSs. The text has been revised by including these potential causes (lines 237-245):

"For Q_1, previous studies (Johnson, 1984; Schumacher et al., 2007) interpreted the double peaks as a result from shallow cumulus in lower level and deep convection or MCS in middle to upper level, although sometimes they superposed as one peak (Johnson, 1984). Moreover, latent cooling due to ice melting in the stratiform region may also contribute to the local minimum of Q_1 which, in some field campaigns, is only shown as an inflection (Johnson et al., 2016). Nevertheless, the local minimum or the inflection usually occurs near the melting level (~600 hPa) in many other tropical field campaigns (e.g. Schumacher et al., 2008; Xie et al., 2010a; Ahmed et al., 2016), indicating that the melting level is nearly constant in the tropics."

Reply to the Interactive comments by Julia Cohen on 13 September, 2016

The publication of this paper is relevant to the understanding of the diurnal cycle of convection in the Amazon region. However it is necessary that some doubtful points listed below are answered in order to accept the publication of this article.

Line 62: Give some reference about this paragraph.

Reply: Relevant references (Harriss et al., 1988; Harriss et al., 1990; Fu et al., 1999; Nobre et al., 2009; Filho et al., 2015) are added in the revised text (Lines 61-63)

Line 202: Greco et al, 1994 also estimated W, Q1 and Q2 for a Squall Line observed during ABLE-2b in the Manaus region. I recommend the authors include this pioneering reference in the Amazon. Compare your results with those found in Greco et al, 1994.

Reply: Thanks for the suggestion. We added this reference and compared the results in lines 223-227:

"Overall, the magnitude of Q_1 and Q_2 are consistent with Schumacher et al. (2007) for LBA at southwestern Brazilian Amazon but much smaller than Greco et al. (1994) at Manaus region. The much larger magnitude in Greco et al. (1994) is likely because it is a case study of one day. The peak height in this study is also lower than the other two studies, indicating that our cases contain more shallow cumulus and convections with low-level heating and drying."

Line 273: Include the paper Greco et al, 1990 which was the first paper that characterized the LOS, BOS and COS in Manaus region (Greco et al 1990).
Reply: revised as suggested.

Line 291: One of the case studies in this paper was called COS as defined by Kouky, 1980; Greco et al, 1990; Cohen et al, 1995. Thus, to be considered as a COS, this convective system must have formed in the afternoon of March 19 along the Atlantic Coast Amazon and crossed by Manaus on March 20 in the morning. Looking at satellite images I realized that actually formed a squall line on the coast in March 19, but duringits propagation inland this convective system lost its linear format and did not reach Manaus region. Therefore, I recommend that the convective system observed March 20 be classified as BOS, since even in the satellite images it does not represent a COS classic. Thus, I ask you to choose one of two cases of BOS to use in this publication.
Reply: We re-examined the radar and satellite images and agree that the March 20 case is classified as BOS. Another COS case on Feb. 21 is chosen for analysis and the numbers of convective systems are also re-counted. Relevant table and figures are revised due to this change (Table 1, Figures 9 and 11). Our main results are not changed due to this revision.

Large-Scale Vertical Velocity, Diabatic Heating and Drying Profiles Associated with Seasonal and Diurnal Variations of Convective Systems Observed in the GoAmazon2014/5 Experiment

Shuaiqi Tang[1], Shaocheng Xie[1], Yunyan Zhang[1], Minghua Zhang[2], Courtney Schumacher[3], Hannah Upton[3], Michael P. Jensen[4], Karen L. Johnson[4], Meng Wang[4], Maike Ahlgrimm[5], Zhe Feng[6], Patrick Minnis[7] and Mandana Thieman[8]

[1]Lawrence Livermore National Laboratory, Livermore, CA, 94550, USA
[2]School of Marine and Atmospheric Sciences, tony Brook University, Stony Brook, NY, 11794, USA
[3]Department of Atmospheric Sciences, Texas A&M University, College Station, TX, 77843, USA
[4]Brookhaven National Laboratory, Upton, NY, 11973, USA
[5]European Centre for Medium-Range Weather Forecasts, Shinfield Park, Reading RG2 9AX, United Kingdom
[6]Pacific Northwest National Laboratory, Richland,Washington, 99354, USA
[7]NASA Langley Research Center, Hampton, VA, 23681, USA
[8]Science Systems and Applications, Inc, Hampton, VA 23666, USA

Correspondence to: Shuaiqi Tang (tang32@llnl.gov)

Abstract. This study describes the characteristics of large-scale vertical velocity, apparent heating source (Q_1) and apparent moisture sink (Q_2) profiles associated with seasonal and diurnal variations of convective systems observed during the two intensive operational periods (IOPs) that was conducted from 15 February to 26 March 2014 (wet season) and from 1 September to 10 October 2014 (dry season) near Manaus, Brazil, during ~~of~~ the Green Ocean Amazon (GoAmazon2014/5) experiment~~, which was conducted near Manaus, Brazil in 2014 and 2015~~. The derived large-scale fields have large diurnal variations according to convective activity in the GoAmazon region and the morning profiles show distinct differences between the dry and wet seasons. In the wet season, propagating convective systems originating far from the GoAmazon region are often seen in the early morning, while in the dry season, they are rarely observed. Afternoon convective systems due to solar heating are frequently seen in both seasons. Accordingly, in the morning, there is strong upward motion and associated heating and drying throughout the entire troposphere in the wet season, which is limited to lower levels in the dry

season. In the afternoon, both seasons exhibit weak heating and strong moistening in the boundary layer related to the vertical convergence of eddy fluxes. A set of case studies of three typical types of convective systems occurring in Amazonia - i.e., locally-occurring systems, coastal-occurring systems and basin-occurring systems - is also conducted to investigate the variability of the large-scale environment with different types of convective systems.

1. Introduction

Amazonia is one of the major tropical convective regions in the global climate system. It provides moisture to the global hydrological cycle and energy to drive the global atmospheric circulation. Understanding convective systems over the Amazon region through observations is important for understanding and simulating global circulation and climate. However, most of Amazonia is covered by tropical forest with only a few observational sites. In order to collect the observations needed to improve our understanding of convective systems over Amazonia, several major field campaigns have been conducted in this area such as the Amazon Boundary Layer Experiments (Harriss et al., 1988; Harriss et al., 1990), the Large-Scale Biosphere-Atmosphere Experiment in Amazonia (LBA) (Silva Dias et al., 2002b), and the CHUVA project (Machado et al., 2014).

Recently, an internationally collaborative experiment, the Observations and Modeling of the Green Ocean Amazon (GoAmazon2014/5) (Martin et al., 2016), was conducted in the region around Manaus, Brazil from January 2014 to December 2015 with a focus on the aerosol and cloud life cycles and aerosol-cloud-precipitation interactions over tropical rainforests. Two 40-day Intensive Operational Periods (IOPs) were conducted in 2014 to investigate the seasonal variations of clouds and aerosols, as well as their interactions. IOP1 took place from 15 February to 26 March 2014 during the wet season, and IOP2 took place from 1 September to 10 October 2014 during the dry season. The goal of this study is to document and understand the seasonal variability and diurnal cycle of large-scale vertical velocity, heat and moisture budgets associated with the convective systems observed during the two IOPs in the GoAmazon2014/5 experiment.

The Amazon region has a significant seasonal variation in precipitation amount. Rainfall is approximately 300 mm per month during the wet season while it is close to 100 mm per month during the dry season (Tanaka et al., 2014). Many studies have examined the seasonal variation of clouds and precipitation in Amazonia ~~(e.g. Fu et al., 2001; Schumacher and Houze, 2003; Machado et al., 2004; Li et al., 2006; Marengo et al., 2012).~~ (e.g. Harriss et al., 1988; Harriss et al., 1990; Fu et al., 1999; Fu et al., 2001; Schumacher and Houze, 2003; Machado et al., 2004; Li et al., 2006; Nobre et al., 2009; Marengo et al., 2012; Filho et al., 2015). Compared to the large variation in clouds and rainfall, the seasonal variation in CAPE is small (Machado et al., 2004; Martin et al., 2016).~~,~~ ~~which implies~~ Martin et al. (2016) suggests that small perturbations in the large-scale circulation can drive dramatic changes in hydrological fields in this region. Few studies, however, have studied the seasonal variation of the diabatic heating and drying structures associated with the convective systems in the Amazon region.

The diurnal cycle of the atmosphere is an important feature that is poorly simulated in climate models. Many efforts have been made to observe and to understand the diurnal cycle over the Amazon basin using surface observations (e.g. Harriss et al., 1990; Cutrim et al., 2000; Machado et al., 2004; Tanaka et al., 2014) or satellite data (e.g. Minnis and Harrison, 1984; Greco et al., 1990; Janowiak et al., 2005; Burleyson et al., 2016). The diurnal cycle over the Amazon basin is complex because it is affected by three types of convective systems: locally-occurring systems (LOS) generated locally in the form of small convective cells (area less than 1000 km^2) with short life time (on the order of 1 hour), coastal-occurring systems (COS) initialized at the northeast coast of Brazil by the sea-breeze and propagating inland as squall lines, and basin-occurring systems (BOS) initialized in the Amazon basin in the form of mesoscale convective systems (MCS) with areas larger than 1000 km^2 (Greco et al., 1990). These systems

reach Manaus, near the center of the Amazon basin, at different times of the day, causing a broad peak of precipitation from morning to early afternoon (e.g. Machado et al., 2004; Tanaka et al., 2014; Burleyson et al., 2016). Schumacher et al. (2007) examined the diurnal cycle of the large-scale ~~Q_1~~ heating budget in the southwest Amazon during LBA, but used only two profiles per day, which do not capture the rapidly changing environment. In addition, the diurnal cycle over the highly deforested southwest Amazon is not necessarily representative of the more pristine central Amazonian rainforest.

In this study we use data collected from the comprehensive GoAmazon2014/5 field campaign to examine the seasonal and diurnal variations of the large-scale vertical velocity and heat and moisture budgets associated with the convective systems that occur in central Amazonia. Section 2 provides details of the data and method used to derive the large-scale profiles for the GoAmazon2014/5 experiment. Section 3 describes the synoptic conditions for the two IOPs. Sections 4 and 5 show the seasonal variation and diurnal cycle of the large-scale fields, respectively. Section 6 further investigates three selected cases representing different types of convective systems in the wet season. The summary and discussion are given in Section 7.

2. Data and Method

Due to the lack of an appropriate sounding array to capture the divergence and advection fields in the analysis domain, the large-scale vertical velocity and budgets analyzed in this study were derived by using, as a first guess, the European Centre for Medium-Range Weather Forecasts (ECMWF) analysis data that are subsequently constrained with domain averaged surface and top of atmosphere (TOA) observations. The upper-level fields from ECMWF

analysis data are adjusted to conserve the vertical integration of mass, moisture and dry static energy through a constrained variational analysis technique described in Zhang and Lin (1997) and Zhang et al. (2001). As indicated in Xie et al. (2004), the use of the surface and TOA observations as constraints improves the quality of the large-scale vertical velocity and budgets in operational analysis data and makes the data suitable for budget analysis and cloud modeling studies. An important by-product of this study is the derived large-scale forcing data (ARM Climate Research Facility, 2001) supporting modeling studies, which are available to the community at the Atmospheric Radiation Measurement (ARM) program Archive (http://iop.archive.arm.gov/arm-iop/0eval-data/xie/scm-forcing/iop_at_mao/).

Figure 1 shows the location of the GoAmazon2014/5 experiment and the analysis domain (the red octagon, referred to as the GoAmazon domain) used in this study, which is about 110 km in radius. The observational research sites and major cities near the region are also shown on the map. The required surface and TOA fluxes as the constraints for the variational analysis are constructed as follows. The precipitation used in this study is derived from the System for the Protection of Amazonia (SIPAM) S-band (10 cm wavelength) radar operated at Ponta Pelada airport, the center of the GoAmazon domain. The SIPAM radar reflectivity constant altitude plan position indicator (CAPPI) at 2.5 km above ground was used to generate the rain rate products using a single Z-R relation of $Z = 174.8R^{1.56}$ derived from Joss-Waldvogel disdrometer data obtained by the CHUVA campaign near Manacapuru during the wet season of early 2014. Other surface constraint variables, such as surface radiative fluxes and latent and sensible heat fluxes, are obtained from the broadband radiometer (ARM Climate Research Facility, 1994) and eddy correlation flux measurement system (ARM Climate Research Facility, 2003) at the ARM Mobile Facility site near Manacapuru (3.213°S, 60.598°W; "ARM site" in Figure 1).

Observations of latent and sensible heat fluxes at two other Brazilian research sites - K34 ("~~FLUXNET-BR-Ma2~~ZF2" in Figure 1) and the Amazon Tall Tower Observatory ("ATTO ~~Tower~~" in Figure 1) - are also used. ~~Because of the limited number of surface sites, it is challenging to obtain domain mean fluxes that can well represent the analysis domain. In this study, we use the Cressman's objective analysis method (Cressman, 1959) to incorporate these limited observations into the analysis with the ECMWF analysis as the first guess.~~ The TOA measurements of broadband radiative fluxes are estimated from the Thirteenth Geostationary Operational Environmental Satellite (GOES-13) 4-km visible (0.65 μm) and infrared window (10.8 μm) radiances using the narrowband-to-broadband (NB-BB) conversion method of Minnis and Smith (1998) that was updated similar to Khaiyer et al. (2010), with some modifications to more closely match those measured by the Clouds and Earth's Radiant Energy System (CERES) on the Aqua and Terra satellite. The radar precipitation and satellite data are 3-hourly average over the analysis domain. The surface radiative fluxes and latent and sensible heat fluxes are first averaged into 3-hour resolution. Then we use the Cressman's objective analysis method (Cressman, 1959) to incorporate these limited number of observations with the ECMWF gridded analysis and calculate the domain mean, so that the domain-mean surface fluxes can better represent the entire domain. The derived large-scale vertical velocity and budgets are thus representing a 3-hour average over analysis domain. The vertical resolution is 25 hPa. ~~All data are interpolated into 3 h and 25 hPa (if applicable) temporal and vertical resolutions, respectively.~~

3. Background of Synoptic Conditions

146 The IOP-averaged sea-level pressure and 10-meter horizontal winds from ERA-Interim
147 reanalysis (Dee et al., 2011) are plotted in Figure 2. During IOP1, the Atlantic Intertropical
148 Convergence Zone (ITCZ) was located near the Equator; while during IOP2, it was located near
149 10°N. A fourteen-day trajectory study shows that the air masses over Manaus typically come
150 from the Northern Hemisphere during IOP1 and from the Southern Hemisphere during IOP2
151 (Martin et al., 2016). The top three rows of Figure 3 show the domain-averaged zonal (u) wind,
152 meridional (v) wind, and relative humidity relative to liquid water, from the adjusted ECMWF
153 analysis. Consistent with those derived from radiosonde data in Martin et al. (2016), IOP1 was
154 dominated by northeasterly winds in the lower troposphere, with moist air throughout the
155 troposphere; IOP2 was dominated by easterly winds in the lower troposphere, with a dry free
156 troposphere.

157 The cloud frequency and domain-mean precipitation observed during IOP1 and IOP2 are
158 shown in the remaining two rows of Figure 3. The cloud frequency was derived from the Active
159 Remote Sensing of Clouds (ARSCL) (Kollias et al., 2007) product, which uses a combination of
160 the 95GHz W-band ARM cloud radar (WACR), micropulse lidar (MPL), and ceilometer located
161 at the ARM site pointing upward to determine a best-estimate cloud mask above the ARM site
162 with 5-second temporal and 30-meter vertical resolution. The ARSCL product leverages each
163 instrument's strengths: the WACR penetrates non-precipitating and weakly precipitating thick
164 clouds, the MPL is sensitive to thin clouds, and the ceilometer reliably detects cloud base. The
165 ARSCL-derived cloud mask data were then used to produce 3-hourly cloud frequencies
166 following the method described in Xie et al. (2010b). The wet season has more cloud and
167 precipitation events than the dry season. However, the convective systems in the dry season are
168 typically more intense than those occurring in the wet season (Giangrande et al., 2016).

169 Compared to 15-year climatology, the precipitation around Manaus during 2014 has a positive
170 anomaly in IOP1 and negative anomaly in IOP2 (Burleyson et al., 2016; Martin et al., 2016).
171 Nevertheless, the annual cycle in 2014 is still broadly representative of the climatology
172 (Burleyson et al., 2016).

173

174 **4. Seasonal Variation**

175 In this section, we focus on the contrast between the dry and wet season large-scale
176 vertical velocity and energy and moisture budgets. The upper row of Figure 4 shows the
177 temporal evolution of large-scale vertical velocity in IOP1 (wet season, left) and IOP2 (dry
178 season, right), and the IOP-mean profiles are shown as the black solid lines in the bottom row.
179 We also define rainy (black dotted lines) and non-rain periods (gray lines) using a threshold of
180 0.2 mm hr^{-1}. A value of 0.2 mm hr^{-1} rather than 0 mm hr^{-1} is used because in some cases ground
181 clutter in the SIPAM radar data may be misinterpreted as light precipitation. Changing the
182 threshold affects the magnitude of the vertical profiles but does not change the seasonal contrast
183 and the results of this study. Using this threshold, the percentage of the rainy period to the entire
184 IOP is 36.9% for IOP1, but is 17.8% for IOP2, indicating that the rain frequency is an important
185 factor impacting the seasonal mean contrast. The red and blue lines represent the mean profiles
186 of morning (at 5 local time (LT)) precipitation systems and afternoon (at 14 LT) precipitation
187 systems, respectively, which will be discussed in Section 5.

188 The non-rain vertical velocity profiles are relatively weak, with downward motion
189 dominating in the upper troposphere during both dry and wet seasons. The rainy vertical
190 velocity profiles show strong upward motion throughout the troposphere during both IOPs, but

191 the level of maximum upward motion is different. The upward motion during the rainy period of
192 IOP1 has a broad peak structure from ~700 to 300 hPa with the maximum at ~350 hPa. The
193 350-hPa upward motion peak is consistent with that shown in the Tropical Ocean and Global
194 Atmosphere Coupled Ocean-Atmosphere Response Experiment (TOGA COARE) (Lin and
195 Johnson, 1996), but lower than the peak of ~265 hPa observed in the Tropical Warm Pool-
196 International Cloud Experiment (TWP-ICE) (Xie et al., 2010a). The upward motion during the
197 IOP2 rainy period also has a broad peak but the maximum is at a much lower level (~550 hPa)
198 than in IOP1. Because the frequency of the rainy period is higher in IOP1 than in IOP2, the IOP-
199 mean upward motion is stronger during IOP1 but weaker and limited to the lower troposphere
200 during IOP2. As discussed in the next section, the difference in morning precipitation systems
201 largely contributes to the seasonal contrast in the vertical velocity profiles between the wet and
202 dry seasons.

203 Figures 5 and 6 show the temporal evolution and IOP-mean of apparent heating Q_1 and
204 apparent drying Q_2 profiles, respectively. Q_1 and Q_2 were first introduced by Yanai et al. (1973)
205 to estimate the diabatic processes:

206
$$\begin{aligned} Q_1 &= \frac{\partial \bar{s}}{\partial t} + \bar{\vec{V}} \cdot \nabla \bar{s} + \bar{\omega} \frac{\partial \bar{s}}{\partial p} \qquad Q_1 = \frac{1}{C_p}\left(\frac{\partial \bar{s}}{\partial t} + \bar{\vec{V}} \cdot \nabla \bar{s} + \bar{\omega} \frac{\partial \bar{s}}{\partial p} \right) \\ &= Q_{rad} + L_v (c - e) - \frac{\partial \overline{\omega' s'}}{\partial p} \qquad = \frac{1}{C_p}\left(Q_{rad} + L_v (c - e) - \frac{\partial \overline{\omega' s'}}{\partial p} \right) \end{aligned} , \quad (1)$$

Field Code Changed

$$Q_2 = -L_v\left(\frac{\partial \bar{q}}{\partial t} + \bar{\vec{V}}\cdot\nabla\bar{q} + \bar{\omega}\frac{\partial \bar{q}}{\partial p}\right) \quad Q_2 = -\frac{L_v}{C_p}\left(\frac{\partial \bar{q}}{\partial t} + \bar{\vec{V}}\cdot\nabla\bar{q} + \bar{\omega}\frac{\partial \bar{q}}{\partial p}\right)$$
$$= L_v\left(c-e\right) + L_v\frac{\partial\overline{\omega' q'}}{\partial p} \qquad = \frac{L_v}{C_p}\left(c-e+\frac{\partial\overline{\omega' q'}}{\partial p}\right) \quad , \tag{2}$$

where $s = C_p T + gz$ is the dry static energy and C_p is the specific heat for dry air in constant pressure; q is water vapor mixing ratio; $\vec{V}$ is horizontal wind vector; ω is vertical velocity in pressure coordinate; Q_{rad} is radiative heating; $L_v\left(c-e\right)$ is the latent heat from water condensation and evaporation (in general it also includes the latent heat and water vapor change from ice phase change); the overbar refers to a horizontal average and the prime refers to a deviation from the average. Q_1 and Q_2 are calculated from the large-scale dynamics (the first lines of the equations) and represent the unresolved physical heat sources and moisture sinks (the second lines). Because the thermodynamic equation and water vapor conservation equation are explicitly satisfied in the variational analysis and the observed precipitation is used as the constraint, the vertical integral of $Q_1 - Q_{rad}$ and vertical integral of Q_2 are consistent with the observed precipitation rate implicitly. The vertical distributions of heating and drying profiles are important to the large-scale circulation as discussed in many other studies (e.g. Hartmann et al., 1984; Lau and Peng, 1987; Puri, 1987; Hack and Schubert, 1990).

Overall, the magnitude of Q_1 and Q_2 are consistent with Schumacher et al. (2007) for LBA at southwestern Brazilian Amazon but much smaller than Greco et al. (1994) at Manaus region. The much larger magnitude in Greco et al. (1994) is likely because it is a case study of one day. The peak height in this study is also lower than the other two studies, indicating that our cases contain more shallow cumulus and convections with low-level heating and drying.

Field Code Changed

Field Code Changed

Field Code Changed

Similar to the profiles of vertical velocity, non-rain Q_1 and Q_2 profile magnitudes in both IOPs are weak with small amounts of heating and moistening below 600 hPa indicative of non-precipitating or very weakly precipitating shallow cumulus and congestus clouds (Schumacher et al., 2008). Rainy period Q_1 and Q_2 profiles show strong heating and drying throughout the troposphere during both IOPs associated with deep convection, and both of them have double peak structures that vary between dry and wet seasons. Q_1 during IOP1 has a broad primary peak between 600 and 400 hPa, while the primary Q_1 peak during IOP2 maximizes more sharply at 550 hPa. The secondary peaks of Q_1 are at ~750 hPa in both IOPs. The peaks of Q_2 in IOP1 (at 500 and 750 hPa) are higher than those in IOP2 (at 650 and 800 hPa). The double peak features of Q_1 and Q_2 are likely due to different physical processes. For Q_1, previous studies (Johnson, 1984; Schumacher et al., 2007) interpreted the double peaks as a result from shallow cumulus in lower level and deep convection or MCS in middle to upper level, although sometimes they superposed as one peak (Johnson, 1984). Moreover, latent cooling due to ice melting in the stratiform region may also contribute to the local minimum of Q_1 which, in some field campaigns, is only shown as an inflection (Johnson et al., 2016). Nevertheless, the local minimum or the inflection usually occurs near the melting level (~600 hPa) in many other tropical field campaigns (e.g. Schumacher et al., 2008; Xie et al., 2010a; Ahmed et al., 2016), indicating that the melting level is nearly constant in the tropics.~~the local minimum usually occurs near the melting level (~600 hPa), indicating latent cooling due to ice melting. Because the melting level is nearly constant in the tropics, the local minimums of Q_1 are more or less at the same level as seen in other tropical field campaigns (e.g. Schumacher et al., 2008; Xie et al., 2010a).~~ For Q_2, the double-peak structure is the combined effect of convective (lower peak) and stratiform (higher peak) rain production (Lin and Johnson, 1996). The peak levels for stratiform

and convective clouds may vary in different locations and times such as in the two IOPs in this study.

5. Diurnal Cycle

The diurnal cycles of domain mean radar-derived precipitation and surface CAPE and convective inhibition (CIN) for both IOPs are plotted in Figure 7. Precipitation in IOP1 extends from early morning to afternoon, consistent with Tanaka et al. (2014). In IOP2, most of the precipitation occurs in the afternoon. The magnitude of afternoon precipitation in IOP2 is just slightly smaller than that in IOP1, but the magnitude of morning precipitation in IOP2 is significantly lower than that in IOP1, indicating that the differences between dry and wet seasons are mainly due to the morning precipitation events. The surface CAPE has similar magnitudes in the daytime during IOP1 and IOP2, but in the early morning it rises later and slower during IOP1 than during IOP2, probably because early morning precipitation during IOP1 has released atmospheric instability. The surface CIN is typically small, especially during IOP1, which is due to the high surface relative humidity over the Amazon rainforest.

The diurnal cycles of cloud frequency, large-scale vertical velocity, Q_1, Q_2 and ~~$Q_1 - Q_2$~~ $Q_1 - Q_2 - Q_{rad}$ for IOP1 (left) and IOP2 (right) are shown in Figure 8. Derived from Eq. (1) and (2),

Field Code Changed

$$\text{~~}Q_1 - Q_2 = Q_{rad} = -\frac{\partial \overline{\omega' h'}}{\partial p}\text{~~} \quad Q_1 - Q_2 - Q_{rad} = -\frac{1}{C_p}\frac{\partial \overline{\omega' h'}}{\partial p} \tag{3}$$

Field Code Changed

where $h = s + L_v q$ is the moist static energy, and Q_{rad} is estimated from using the radiative transfer model in the single-column model of CAM5 (Neale et al., 2012) driven by the large-scale forcing data derived from this study since it cannot be directly measured and retrievals for Q_{rad} using observed vertical cloud profiles (Feng et al., 2014) have not been available yet. . With the ~~phase change of water vapor cancelled~~freezing and melting processes ignored, $Q_1 - Q_2 - Q_{rad}$ ~~$Q_1 - Q_2$~~ represents the ~~radiative effect and the~~ vertical convergence of ~~eddy fluxes~~ h by sub-grid turbulence and cumulus.

Field Code Changed

Field Code Changed

Field Code Changed

Consistent with the diurnal cycles of precipitation, the observed clouds and large-scale vertical velocity differ primarily in the morning between IOP1 and IOP2. In IOP1, the early morning upward motion peaks at 700 hPa and extends to the upper troposphere around 200 hPa. The early afternoon upward motion peaks at the upper troposphere and extends above 100 hPa. Accordingly, clouds are mainly seen between 800 and 500 hPa in the early morning but throughout the entire troposphere in the afternoon. In IOP2, morning convective systems are generally limited to the lower levels, as shown by weak upward motion below 600 hPa and downward motion above. Thus, few clouds are observed in the lower and middle troposphere while some high clouds remain from the previous day's convective activities. The afternoon convective systems are strong and deep in both IOPs, with upward motion in the upper troposphere associated with convective cloud growth and downward motion in the lower troposphere associated with convective downdrafts.

Consistent with the clouds and vertical velocity, Figure 8 also shows significant seasonal differences of Q_1 and Q_2 profiles in the morning, with heating and drying extending to the upper troposphere in IOP1 but cooling and moistening above 600-650 hPa in IOP2. In the afternoon,

both IOPs show strong heating and drying in the middle and upper troposphere with weak heating and strong moistening occurring below 700 hPa. The low-level heating and moistening feature has been observed in trade wind regimes during westerly wind bursts and monsoon break periods (Nitta and Esbensen, 1974; Lin and Johnson, 1996; Johnson and Lin, 1997; Xie et al., 2010a), in which the vertical convergence of eddy fluxes and detrainment of shallow cumulus were considered as the causes. In this study it is also seen in the afternoon precipitating periods (red lines in Figure 5 and 6). To further investigate this feature, $Q_1 - Q_2 - Q_{rad}$ is shown in t~~T~~he last row of~~in~~ Figure 8. ~~shows $Q_1 - Q_2$ where t~~T~~wo positive $Q_1 - Q_2 - Q_{rad}$ centers are seen during daytime at ~750 to 950 hPa and ~250 to 550 hPa, respectively. ~~Considering the two terms in the right-hand-side of Eq. (3)~~It is likely that the positive $Q_1 - Q_2 - Q_{rad}$ in the lower level (below 600 hPa) is mainly due to the vertical convergence of h by boundary layer turbulence and shallow cumulus. The positive $Q_1 - Q_2 - Q_{rad}$ in the upper troposphere (above 600 hPa) may be due to the vertical convergence of h by deep convective process. Note that $Q_1 - Q_2 - Q_{rad}$ also includes latent heat from ice freezing and melting, which may contribute to the local minimum around 600 hPa.~~, the troposphere usually has a radiative cooling effect and therefore Q_{rad} is usually negative. The positive $Q_1 - Q_2$ has to be due to the vertical convergence of eddy fluxes of moist static energy associated with convective process, where positive Q_1 comes from vertical convergence of dry static energy flux, and negative Q_2 comes from vertical convergence of moisture flux.~~

Field Code Changed

Field Code Changed

Field Code Changed

Formatted: Font: Italic

Field Code Changed

Formatted: Font: Italic

Field Code Changed

6. Case Studies

A set of case studies is conducted to further understand the large-scale vertical velocity and heat and moisture budgets for the three typical types of convective systems (Greco et al., 1990) that often occur in the wet season in Amazonia: locally-occurring systems (LOS), coastal-occurring systems (COS), and basin-occurring systems (BOS). Previous studies have found that LOS often occur in the afternoon characterized as scattered convections generated through solar heating at the surface, while most COS and BOS are propagating systems associated with mid-level easterlies and westerlies, respectively (e.g. Cifelli et al., 2002; Silva Dias et al., 2002a; Williams et al., 2002), and affect Manaus in the early morning. COS occurring in easterlies are often westward propagating squall-lines with intense leading lines that are more vertically developed. BOS generated in the westerlies are generally less vertically developed MCSs with a broad horizontal area and relatively homogeneous precipitation extending over a long time (Cifelli et al., 2002). Table 1 gives the number of each type of precipitation system observed during the two IOPs, identified from the radar loop (available at https://www.youtube.com/playlist?list=PLVqbwaasmlvtcu2kl_U5RaaNF0kYqW6ua) and the satellite infrared images (available at http://www-pm.larc.nasa.gov/). ~~The two BOS cases identified in IOP2 both occurred in the Amazon basin, but~~There are some cases in the easterlies identified as BOS because they initiated in the Amazon basin but their structures are more like COS as squall lines ~~propagating westward~~. ~~There are m~~More COS and BOS are seen in IOP1 than in IOP2, but the number of afternoon LOS in IOP1 is just slightly higher than that in IOP2. This again indicates that the frequency of morning propagating convective systems contributes to the variation of the diurnal cycle between the wet and dry seasons.

The three selected cases are a LOS starting from 11 LT, 13 March 2014, a COS starting from ~~2~~23 LT, 20 ~~March~~ February 2014 and a BOS starting from 17 LT, 1 March 2014. The

337 times of these events are marked by the black lines in Figure 3. Mid-level wind was dominated
338 by westerlies on 1 March (day 60) and easterlies on 20 ~~March~~ February (day ~~79~~51). Figure 9
339 shows representative scans of the radar reflectivity at elevation angle of 0.9° for these three cases,
340 as well as the time series of the domain mean precipitation. The LOS case has many small-scale
341 scattered convective cells that last for very short times (typically a couple of hours). Because of
342 the small horizontal coverage of the convective cells, the domain mean precipitation is less than
343 that in the other two cases. The COS case has a clear bow-shape echo indicating a squall line
344 front~~. The horizontal size of the precipitating system is about 100 km and it~~ which moves
345 quickly westward. The BOS case has a ~~much~~ larger horizontal area of moderate precipitation
346 with some embedded convective cells. It moves southeastward and lasts more than 10 hours
347 over the GoAmazon domain.

348 The point-observed cloud frequency and domain-averaged relative humidity, surface
349 CAPE and CIN, u- and v-winds, ~~relative humidity,~~ large-scale vertical velocity, Q_1, ~~and~~ Q_2 and
350 $Q_1 - Q_2 - Q_{rad}$ for the three cases are shown in Figures 10-12, respectively. For the LOS case,
351 the cloud frequency is much smaller than in the other two cases, since the convective cells have
352 small horizontal extent and only occupy a small portion of the region. A shallow-to-deep
353 transition of convective clouds can be seen. The surface CAPE is large, with weak mid-level
354 winds and moist air at the surface before the convection occurred. Upward motion corresponds
355 to the deep convection, and the magnitude is smaller than in the other two cases, consistent with
356 weaker precipitation. Starting around 9 LT, Q_1 shows diabatic heating throughout the
357 troposphere during the deep convection, while Q_2 shows strong moistening between 750 and 950
358 hPa and weak drying above that layer. The daytime positive $Q_1 - Q_2 - Q_{rad}$ ~~moistening~~ between
359 750 and 950 hPa is mainly contributed by negative Q_2 representing ~~due to the~~ vertical

Field Code Changed

Field Code Changed

convergence of ~~eddy moisture fluxes~~moisture by sub-grid eddies. It can also be seen on many other days during the two IOPs and are similar to the daytime profiles discussed in the diurnal cycle (Section 5) ~~and was discussed in Section 5~~. Note that there is a time lag between observed cloud frequency and the domain-averaged large-scale fields, which might be partially due to the fact that the cloud frequency observations were taken from vertically pointing instruments at the ARM site 67.8 km downwind of the center of the GoAmazon domain.

The COS (Figure 11) and BOS (Figure 12) cases both show a shallow-to-deep convective cloud transition from the previous evening to late afternoon, with a moist lower-level atmosphere. Both cases have smaller surface CAPE than the LOS case, possibly because the convective systems have released the atmospheric instability in the morning. The COS case passed through the GoAmazon domain ~~between 6 and 12~~around 6 LT in strong mid-level easterlies, with deep clouds and strong upward motion associated with the squall line. Stratiform clouds, associated with weak upward motion, remained in the upper levels until ~~~16~~ 18 LT. Condensation from the deep convection contributes to strong diabatic heating and drying throughout the troposphere, while after the passage of the squall line (12-18 LT),~~-~~there are some stratiform clouds remaining indicated by upper-level heating/drying and lower-level cooling/moistening. ~~a few isolated convective cells moved in and the large-scale structure becomes similar to that in the LOS case, with upper-level heating and drying, low-level heating and moistening.~~ The BOS case entered the GoAmazon domain earlier than the COS case. In weak mid-level westerlies and descending mid-to-low-level northerlies, the system moved slowly southeastward and remained in the domain for a longer time. Strong upward motion related to the MCS is seen from 18 to 6 LT. Large diabatic heating and drying related to the strong condensation is also seen. The remnant high clouds were maintained until ~18 LT with precipitation weakening over time. The upper-

level heating and drying, lower-level cooling and moistening indicate that there are precipitating stratiform clouds in the upper level and evaporation of precipitation underneath. The negative $Q_1 - Q_2 - Q_{rad}$ in the lower level and the positive $Q_1 - Q_2 - Q_{rad}$ in the upper level are seen in both the COS and BOS case, which indicates lower-level divergence of *h* and upper-level convergence of *h* due to moist convective processes, consistent with Tang and Zhang (2015). The lower-level positive $Q_1 - Q_2 - Q_{rad}$ in the afternoon is mainly contributed by the vertical convergence of moisture by sub-grid eddies, similar to that in the LOS case.

Field Code Changed

Field Code Changed

Field Code Changed

7. Summary and Discussion

This study presented the characteristics of the seasonal variation and diurnal cycle of the large-scale vertical velocity and diabatic heating (Q_1) and drying (Q_2) profiles for the two IOPs conducted during the GoAmazon2014/5 experiment. A constrained variational analysis method was used to derive the large-scale vertical velocity and Q_1 and Q_2 profiles based on surface and TOA observations and ECMWF analysis. The derived profiles correspond well with observed clouds and precipitation describing convective systems over Amazonia.

The large-scale environment over the region near Manaus has distinct seasonal variations and diurnal cycles. The wet season (IOP1) has more frequent precipitation events than the dry season (IOP2), especially in the morning. The large-scale upward motions during rainy periods have similar strength in both IOPs, however, the peak level in IOP1 is much higher than that exhibited in IOP2 (350 hPa vs. 550 hPa). Q_1 and Q_2 both have a double-peak feature during rainy period, but the physical mechanism may be different: the double peak of Q_1 may be due to the combination of shallow and deep convections and latent cooling near the melting level, while

405 the double peak of Q_2 may be due to the different height of convective and stratiform systems.
406 The seasonal contrast is mainly due to the higher occurrence of morning mesoscale convective
407 systems observed during IOP1. In the morning, upward motion peaks at ~700 hPa and extends
408 to the upper troposphere during IOP1, while it is limited to the lower levels with downward
409 motion at the upper levels during IOP2. Afternoon convective systems have a higher vertical
410 motion peak than their morning counterparts, and both IOPs show similar vertical structures for
411 the afternoon systems. The large-scale vertical velocity shows upward motion above 700 hPa and
412 downward motion below. Accordingly, Q_1 and Q_2 also exhibit middle and upper level heating
413 and drying related to the deep convection. Below 750 hPa, the profiles show relatively weak
414 heating and strong moistening. This heating and moistening feature is due to the vertical
415 convergence of ~~eddy fluxes of~~ heat and moisture by sub-grid eddies in the boundary layer.

416 Three cases from IOP1 representing different types of convective systems that often
417 occur in the region were chosen and analyzed in this study: locally-occurring systems (LOS),
418 coastal-occurring systems (COS) and basin-occurring systems (BOS). The LOS case was
419 characterized by many scattered and short-lived convective cells. It had relatively weak upward
420 motion, heating and drying in the free troposphere, and heating and moistening in the boundary
421 layer. The COS case occurred in strong mid-level easterlies. It was characterized as a squall line
422 with deep strong profiles of upward motion, heating and drying. The BOS case mainly happened
423 in weak mid-level westerlies and descending mid-to-low-level northerlies. It was characterized
424 as widespread, moderate precipitation with embedded convective cells, and lasted much longer
425 than the other two systems. The precipitating stratiform clouds remained at upper levels for
426 several hours evident by upper-level condensational heating and lower-level evaporative cooling.
427 The frequency of LOS cases is similar in both IOPs while the COS and BOS events occur much

more often during the wet season than the dry season. The seasonal variation of the diurnal cycle of precipitation, clouds, and environmental variables is mainly due to the COS and BOS events observed in the morning.

Previous studies have also shown that the river breeze has an important influence on the diurnal cycle near the Amazon River (e.g. dos Santos et al., 2014; Tanaka et al., 2014; Burleyson et al., 2016) and that the impact of the local circulation can extend as far as 50 km away from the river. This local circulation and the horizontal inhomogeneity of large-scale vertical velocity, heating, and moistening could be better studied using high-resolution 3-D gridded large-scale forcing data from the three-dimensional constrained variational analysis recently developed by Tang and Zhang (2015) and Tang et al. (2016). This will be the subject of a future study.

Acknowledgment: The authors gratefully thank Luiz Machado, Jiwen Fan and many others in the GoAmazon group for valuable discussions about the synoptic and climate features in Amazonia region. This research is supported by the Biological and Environmental Research Division in the Office of Sciences of the US Department of Energy (DOE). Work at LLNL was supported by the DOE Atmospheric Radiation Measurement (ARM) program and performed under the auspices of the U. S. Department of Energy by Lawrence Livermore National Laboratory under contract No. DE-AC52-07NA27344. Work at Stony Brook was supported by the Office of Science of the U. S. Department of Energy and by the National Science Foundation. This manuscript has been authored by employees of Brookhaven Science Associates, LLC with support from the ARM program and Atmospheric Systems Research Program under Contract No. DE-AC02-98CH10886 with the U.S. Department of Energy. Dr. Zhe Feng at the Pacific

Northwest National Laboratory (PNNL) is supported by the U.S. DOE, as part of the Atmospheric System Research (ASR) Program. PNNL is operated for DOE by Battelle Memorial Institute under contract DE-AC05-76RL01830. Work at ECMWF was supported by the U. S. Department of Energy via the Atmospheric Systems Research Program under Contract No. DE-SC0005259. The satellite analyses are supported by the DOE ARM and ASR Program sunder contract, DE-SC0013896. The publisher by accepting the manuscript for publication acknowledges that the United States Government retains a non-exclusive, paid-up, irrevocable, world-wide license to publish or reproduce the published form of this manuscript, or allow others to do so, for United States Government purposes. We thank The Brazilian National Institute of Amazonian Research (INPA), the Amazonas State University (UEA) and Dr. Antonio Manzi for providing surface flux data.

461 **References**

462 Ahmed, F., Schumacher, C., Feng, Z., and Hagos, S.: A Retrieval of Tropical Latent Heating
463 Using the 3D Structure of Precipitation Features, Journal of Applied Meteorology and
464 Climatology, 55, 1965-1982, doi: doi:10.1175/JAMC-D-15-0038.1, 2016.

465 Atmospheric Radiation Measurement (ARM) Climate Research Facility, updated hourly.
466 Radiative Flux Analysis (RADFLUX1LONG). 2014-02-15 to 2014-10-10, 3.21297 S 60.5981
467 W: ARM Mobile Facility (MAO) Manacapuru, Amazonas, Brazil; AMF1 (M1). Compiled by C.
468 Long, K. Gaustad and L. Riihimaki. Atmospheric Radiation Measurement (ARM) Climate
469 Research Facility Data Archive: Oak Ridge, Tennessee, USA. Data set accessed 2016-03-09 at
470 doi: 10.5439/1179822, 1994.

471 Atmospheric Radiation Measurement (ARM) Climate Research Facility, updated monthly.
472 SCM-Forcing DATA from variational analysis (VARANAL). 2014-02-18 to 2014-10-10,
473 3.21297 S 60.5981 W: ARM Mobile Facility (MAO) Manacapuru, Amazonas, Brazil; AMF1
474 (M1). Compiled by S. Tang, S. Xie and Y. Zhang. Atmospheric Radiation Measurement (ARM)
475 Climate Research Facility Data Archive: Oak Ridge, Tennessee, USA. Data set accessed 2016-
476 07-22 at doi: 10.5439/1273323.

477 Atmospheric Radiation Measurement (ARM) Climate Research Facility, updated hourly. Quality
478 Controlled Eddy Correlation Flux Measurement (30QCECOR). 2014-02-15 to 2014-10-10,
479 3.21297 S 60.5981 W: ARM Mobile Facility (MAO) Manacapuru, Amazonas, Brazil; AMF1
480 (M1). Compiled by R. McCoy, Y. Zhang and S. Xie. Atmospheric Radiation Measurement
481 (ARM) Climate Research Facility Data Archive: Oak Ridge, Tennessee, USA. Data set accessed
482 2016-03-22 at doi: 10.5439/1097546, 2003.

483 Burleyson, C. D., Feng, Z., Hagos, S., Fast, J., Machado, L. A. T., and Martin, S. T.: Spatial
484 variability of the background diurnal cycle of deep convection around the GoAmazon2014/5
485 field campaign sites, journal of applied Meteorology and Climatology, in revision, doi, 2016.

486 Cifelli, R., Petersen, W. A., Carey, L. D., Rutledge, S. A., and da Silva Dias, M. A. F.: Radar
487 observations of the kinematic, microphysical, and precipitation characteristics of two MCSs in
488 TRMM LBA, Journal of Geophysical Research: Atmospheres, 107, LBA 44-41-LBA 44-16, doi:
489 10.1029/2000JD000264, 2002.

490 Cressman, G. P.: AN OPERATIONAL OBJECTIVE ANALYSIS SYSTEM, Monthly Weather
491 Review, 87, 367-374, doi: doi:10.1175/1520-0493(1959)087<0367:AOOAS>2.0.CO;2, 1959.

492 Cutrim, E. M. C., Martin, D. W., Butzow, D. G., Silva, I. M., and Yulaeva, E.: Pilot Analysis of
493 Hourly Rainfall in Central and Eastern Amazonia, Journal of Climate, 13, 1326-1334, doi:
494 10.1175/1520-0442(2000)013<1326:PAOHRI>2.0.CO;2, 2000.

Dee, D. P., Uppala, S. M., Simmons, A. J., Berrisford, P., Poli, P., Kobayashi, S., Andrae, U., Balmaseda, M. A., Balsamo, G., Bauer, P., Bechtold, P., Beljaars, A. C. M., van de Berg, L., Bidlot, J., Bormann, N., Delsol, C., Dragani, R., Fuentes, M., Geer, A. J., Haimberger, L., Healy, S. B., Hersbach, H., Hólm, E. V., Isaksen, L., Kållberg, P., Köhler, M., Matricardi, M., McNally, A. P., Monge-Sanz, B. M., Morcrette, J. J., Park, B. K., Peubey, C., de Rosnay, P., Tavolato, C., Thépaut, J. N., and Vitart, F.: The ERA-Interim reanalysis: configuration and performance of the data assimilation system, Quarterly Journal of the Royal Meteorological Society, 137, 553-597, doi: 10.1002/qj.828, 2011.

dos Santos, M. J., Silva Dias, M. A. F., and Freitas, E. D.: Influence of local circulations on wind, moisture, and precipitation close to Manaus City, Amazon Region, Brazil, Journal of Geophysical Research: Atmospheres, 119, 13,233-213,249, doi: 10.1002/2014JD021969, 2014.

Feng, Z., McFarlane, S. A., Schumacher, C., Ellis, S., Comstock, J., and Bharadwaj, N.: Constructing a Merged Cloud-Precipitation Radar Dataset for Tropical Convective Clouds during the DYNAMO/AMIE Experiment at Addu Atoll, J. Atmos. Oceanic Technol., 31, 1021-1042, doi: 10.1175/JTECH-D-13-00132.1, 2014.

Filho, A. J. P., Carbone, R. E., Tuttle, J. D., and Karam, H. A.: Convective Rainfall in Amazonia and Adjacent Tropics, Atmospheric and Climate Sciences, 5, 137-161, doi: 10.4236/acs.2015.52011, 2015.

Fu, R., Zhu, B., and Dickinson, R. E.: How Do Atmosphere and Land Surface Influence Seasonal Changes of Convection in the Tropical Amazon?, Journal of Climate, 12, 1306-1321, doi: doi:10.1175/1520-0442(1999)012<1306:HDAALS>2.0.CO;2, 1999.

Fu, R., Dickinson, R. E., Chen, M., and Wang, H.: How Do Tropical Sea Surface Temperatures Influence the Seasonal Distribution of Precipitation in the Equatorial Amazon?, Journal of Climate, 14, 4003-4026, doi: doi:10.1175/1520-0442(2001)014<4003:HDTSST>2.0.CO;2, 2001.

Giangrande, S., Toto, T., Jensen, M. P., Bartholomew, M., Feng, Z., Protat, A., Williams, C., Schumacher, C., and Machado, L.: Convective Cloud Vertical Velocity and Mass-Flux Characteristics from Radar Wind Profiler Observations During GoAmazon2014/5, Journal of Geophysical Research: Atmospheres, in review, doi, 2016.

Greco, S., Swap, R., Garstang, M., Ulanski, S., Shipham, M., Harriss, R. C., Talbot, R., Andreae, M. O., and Artaxo, P.: Rainfall and surface kinematic conditions over central Amazonia during ABLE 2B, Journal of Geophysical Research: Atmospheres, 95, 17001-17014, doi: 10.1029/JD095iD10p17001, 1990.

Greco, S., Scala, J., Halverson, J., Jr., H. L. M., Tao, W.-K., and Garstang, M.: Amazon Coastal Squall Lines. Part II: Heat and Moisture Transports, Monthly Weather Review, 122, 623-635, doi: doi:10.1175/1520-0493(1994)122<0623:ACSLPI>2.0.CO;2, 1994.

Hack, J. J., and Schubert, W. H.: Some dynamical properties of idealized thermally-forced meridional circulations in the tropics, Meteorl. Atmos. Phys., 44, 101-117, doi: 10.1007/BF01026813, 1990.

Harriss, R. C., Wofsy, S. C., Garstang, M., Browell, E. V., Molion, L. C. B., McNeal, R. J., Hoell, J. M., Bendura, R. J., Beck, S. M., Navarro, R. L., Riley, J. T., and Snell, R. L.: The Amazon Boundary Layer Experiment (ABLE 2A): dry season 1985, Journal of Geophysical Research: Atmospheres, 93, 1351-1360, doi: 10.1029/JD093iD02p01351, 1988.

Harriss, R. C., Garstang, M., Wofsy, S. C., Beck, S. M., Bendura, R. J., Coelho, J. R. B., Drewry, J. W., Hoell, J. M., Matson, P. A., McNeal, R. J., Molion, L. C. B., Navarro, R. L., Rabine, V., and Snell, R. L.: The Amazon Boundary Layer Experiment: Wet season 1987, Journal of Geophysical Research: Atmospheres, 95, 16721-16736, doi: 10.1029/JD095iD10p16721, 1990.

Hartmann, D. L., Hendon, H. H., and Houze, R. A.: Some Implications of the Mesoscale Circulations in Tropical Cloud Clusters for Large-Scale Dynamics and Climate, Journal of the Atmospheric Sciences, 41, 113-121, doi: 10.1175/1520-0469(1984)041<0113:SIOTMC>2.0.CO;2, 1984.

Janowiak, J. E., Kousky, V. E., and Joyce, R. J.: Diurnal cycle of precipitation determined from the CMORPH high spatial and temporal resolution global precipitation analyses, Journal of Geophysical Research: Atmospheres, 110, n/a-n/a, doi: 10.1029/2005JD006156, 2005.

Johnson, R. H.: Partitioning Tropical Heat and Moisture Budgets into Cumulus and Mesoscale Components: Implications for Cumulus Parameterization, Monthly Weather Review, 112, 1590-1601, doi: 10.1175/1520-0493(1984)112<1590:PTHAMB>2.0.CO;2, 1984.

Johnson, R. H., and Lin, X.: Episodic Trade Wind Regimes over the Western Pacific Warm Pool, Journal of the Atmospheric Sciences, 54, 2020-2034, doi: 10.1175/1520-0469(1997)054<2020:ETWROT>2.0.CO;2, 1997.

Johnson, R. H., Ciesielski, P. E., and Rickenbach, T. M.: A Further Look at Q1 and Q2 from TOGA COARE, Meteorological Monographs, 56, 1.1-1.12, doi: doi:10.1175/AMSMONOGRAPHS-D-15-0002.1, 2016.

Khaiyer, M., Minnis, P., Doelling, D. R., Nordeen, M. L., Palikonda, R., Rutan, D. A., and Yi, Y.: Improved TOA broadband shortwave and longwave fluxes derived from satellites over the Tropical Western Pacific, 13th Conference on Atmospheric Radiation, Am. Meteorol. Soc., Portland, OR. 27 June to 2 July, 2010.

Kollias, P., Miller, M. A., Luke, E. P., Johnson, K. L., Clothiaux, E. E., Moran, K. P., Widener, K. B., and Albrecht, B. A.: The Atmospheric Radiation Measurement Program Cloud Profiling Radars: Second-Generation Sampling Strategies, Processing, and Cloud Data Products, Journal of Atmospheric and Oceanic Technology, 24, 1199-1214, doi: 10.1175/JTECH2033.1, 2007.

565 Lau, K. M., and Peng, L.: Origin of Low-Frequency (Intraseasonal) Oscillations in the Tropical
566 Atmosphere. Part I: Basic Theory, Journal of the Atmospheric Sciences, 44, 950-972, doi:
567 10.1175/1520-0469(1987)044<0950:OOLFOI>2.0.CO;2, 1987.

568 Li, W., Fu, R., and Dickinson, R. E.: Rainfall and its seasonality over the Amazon in the 21st
569 century as assessed by the coupled models for the IPCC AR4, Journal of Geophysical Research:
570 Atmospheres, 111, n/a-n/a, doi: 10.1029/2005JD006355, 2006.

571 Lin, X., and Johnson, R. H.: Heating, Moistening, and Rainfall over the Western Pacific Warm
572 Pool during TOGA COARE, Journal of the Atmospheric Sciences, 53, 3367-3383, doi:
573 10.1175/1520-0469(1996)053<3367:HMAROT>2.0.CO;2, 1996.

574 Machado, L. A. T., Laurent, H., Dessay, N., and Miranda, I.: Seasonal and diurnal variability of
575 convection over the Amazonia: A comparison of different vegetation types and large scale
576 forcing, Theor Appl Climatol, 78, 61-77, doi: 10.1007/s00704-004-0044-9, 2004.

577 Machado, L. A. T., Silva Dias, M. A. F., Morales, C., Fisch, G., Vila, D., Albrecht, R., Goodman,
578 S. J., Calheiros, A. J. P., Biscaro, T., Kummerow, C., Cohen, J., Fitzjarrald, D., Nascimento, E.
579 L., Sakamoto, M. S., Cunningham, C., Chaboureau, J.-P., Petersen, W. A., Adams, D. K.,
580 Baldini, L., Angelis, C. F., Sapucci, L. F., Salio, P., Barbosa, H. M. J., Landulfo, E., Souza, R. A.
581 F., Blakeslee, R. J., Bailey, J., Freitas, S., Lima, W. F. A., and Tokay, A.: The Chuva Project:
582 How Does Convection Vary across Brazil?, Bulletin of the American Meteorological Society, 95,
583 1365-1380, doi: 10.1175/BAMS-D-13-00084.1, 2014.

584 Marengo, J. A., Liebmann, B., Grimm, A. M., Misra, V., Silva Dias, P. L., Cavalcanti, I. F. A.,
585 Carvalho, L. M. V., Berbery, E. H., Ambrizzi, T., Vera, C. S., Saulo, A. C., Nogues-Paegle, J.,
586 Zipser, E., Seth, A., and Alves, L. M.: Recent developments on the South American monsoon
587 system, International Journal of Climatology, 32, 1-21, doi: 10.1002/joc.2254, 2012.

588 Martin, S. T., Artaxo, P., Machado, L. A. T., Manzi, A. O., Souza, R. A. F., Schumacher, C.,
589 Wang, J., Andreae, M. O., Barbosa, H. M. J., Fan, J., Fisch, G., Goldstein, A. H., Guenther, A.,
590 Jimenez, J. L., Pöschl, U., Silva Dias, M. A., Smith, J. N., and Wendisch, M.: Introduction:
591 Observations and Modeling of the Green Ocean Amazon (GoAmazon2014/5), Atmos. Chem.
592 Phys., 16, 4785-4797, doi: 10.5194/acp-16-4785-2016, 2016.

593 Minnis, P., and Harrison, E. F.: Diurnal Variability of Regional Cloud and Clear-Sky Radiative
594 Parameters Derived from GOES Data. Part II: November 1978 Cloud Distributions, Journal of
595 Climate and Applied Meteorology, 23, 1012-1031, doi: doi:10.1175/1520-
596 0450(1984)023<1012:DVORCA>2.0.CO;2, 1984.

597 Minnis, P., and Smith, W. L.: Cloud and radiative fields derived from GOES-8 during SUCCESS
598 and the ARM-UAV spring 1996 flight series, Geophysical Research Letters, 25, 1113-1116, doi:
599 10.1029/98GL00301, 1998.

600 Neale, R. B., Chen, C.-C., Gettelman, A., Lauritzen, P. H., Park, S., williamson, d., conley, a.,
601 Garcia, R., Kinnison, D., Lamarque, J., Marsh, D., Mills, M., Smith, A., Tilmes, S., Vitt, F.,
602 Morrison, H., Cameron-Smith, P., Collins, W. D., Iacono, M., Easter, R., Ghan, S. J., Liu, X.,
603 Rasch, P. J., and Taylor, M. A.: Description of the NCAR Community Atmosphere Model
604 (CAM 5.0), NCAR Technical Note NCARTN-4861STR, 274, 2012.

605 Nitta, T., and Esbensen, S.: Heat and Moisture Budget Analyses Using BOMEX Data, Monthly
606 Weather Review, 102, 17-28, doi: 10.1175/1520-0493(1974)102<0017:HAMBAU>2.0.CO;2,
607 1974.

608 Nobre, C. A., Obregón, G. O., Marengo, J. A., Fu, R., and Poveda, G.: Characteristics of
609 Amazonian Climate: Main Features, in: Amazonia and Global Change, American Geophysical
610 Union, 149-162, 2009.

611 Puri, K.: Some Experiments on the Use of Tropical Diabatic Heating Information for Initial State
612 Specification, Monthly Weather Review, 115, 1394-1406, doi: 10.1175/1520-
613 0493(1987)115<1394:SEOTUO>2.0.CO;2, 1987.

614 Schumacher, C., and Houze, R. A.: Stratiform Rain in the Tropics as Seen by the TRMM
615 Precipitation Radar*, Journal of Climate, 16, 1739-1756, doi: 10.1175/1520-
616 0442(2003)016<1739:SRITTA>2.0.CO;2, 2003.

617 Schumacher, C., Zhang, M. H., and Ciesielski, P. E.: Heating Structures of the TRMM Field
618 Campaigns, Journal of the Atmospheric Sciences, 64, 2593-2610, doi: 10.1175/JAS3938.1, 2007.

619 Schumacher, C., Ciesielski, P. E., and Zhang, M. H.: Tropical Cloud Heating Profiles: Analysis
620 from KWAJEX, Monthly Weather Review, 136, 4289-4300, doi: 10.1175/2008MWR2275.1,
621 2008.

622 Silva Dias, M. A. F., Petersen, W., Silva Dias, P. L., Cifelli, R., Betts, A. K., Longo, M., Gomes,
623 A. M., Fisch, G. F., Lima, M. A., Antonio, M. A., and Albrecht, R. I.: A case study of convective
624 organization into precipitating lines in the Southwest Amazon during the WETAMC and
625 TRMM-LBA, Journal of Geophysical Research: Atmospheres, 107, LBA 46-41-LBA 46-23, doi:
626 10.1029/2001JD000375, 2002a.

627 Silva Dias, M. A. F., Rutledge, S., Kabat, P., Silva Dias, P. L., Nobre, C., Fisch, G., Dolman, A.
628 J., Zipser, E., Garstang, M., Manzi, A. O., Fuentes, J. D., Rocha, H. R., Marengo, J., Plana-
629 Fattori, A., Sá, L. D. A., Alvalá, R. C. S., Andreae, M. O., Artaxo, P., Gielow, R., and Gatti, L.:
630 Cloud and rain processes in a biosphere-atmosphere interaction context in the Amazon Region,
631 Journal of Geophysical Research: Atmospheres, 107, LBA 39-31-LBA 39-18, doi:
632 10.1029/2001JD000335, 2002b.

633 Tanaka, L. M. d. S., Satyamurty, P., and Machado, L. A. T.: Diurnal variation of precipitation in
634 central Amazon Basin, International Journal of Climatology, 34, 3574-3584, doi:
635 10.1002/joc.3929, 2014.

636 Tang, S., and Zhang, M.: Three-dimensional constrained variational analysis: Approach and
637 application to analysis of atmospheric diabatic heating and derivative fields during an ARM SGP
638 intensive observational period, Journal of Geophysical Research: Atmospheres, 120, 7283-7299,
639 doi: 10.1002/2015JD023621, 2015.

640 Tang, S., Zhang, M., and Xie, S.: An ensemble constrained variational analysis of atmospheric
641 forcing data and its application to evaluate clouds in CAM5, Journal of Geophysical Research:
642 Atmospheres, 121, 33-48, doi: 10.1002/2015JD024167, 2016.

643 Williams, E., Rosenfeld, D., Madden, N., Gerlach, J., Gears, N., Atkinson, L., Dunnemann, N.,
644 Frostrom, G., Antonio, M., Biazon, B., Camargo, R., Franca, H., Gomes, A., Lima, M., Machado,
645 R., Manhaes, S., Nachtigall, L., Piva, H., Quintiliano, W., Machado, L., Artaxo, P., Roberts, G.,
646 Renno, N., Blakeslee, R., Bailey, J., Boccippio, D., Betts, A., Wolff, D., Roy, B., Halverson, J.,
647 Rickenbach, T., Fuentes, J., and Avelino, E.: Contrasting convective regimes over the Amazon:
648 Implications for cloud electrification, Journal of Geophysical Research: Atmospheres, 107, LBA
649 50-51-LBA 50-19, doi: 10.1029/2001JD000380, 2002.

650 Xie, S., Cederwall, R. T., and Zhang, M.: Developing long-term single-column model/cloud
651 system–resolving model forcing data using numerical weather prediction products constrained by
652 surface and top of the atmosphere observations, Journal of Geophysical Research, 109, doi:
653 10.1029/2003jd004045, 2004.

654 Xie, S., Hume, T., Jakob, C., Klein, S. A., McCoy, R. B., and Zhang, M.: Observed Large-Scale
655 Structures and Diabatic Heating and Drying Profiles during TWP-ICE, Journal of Climate, 23,
656 57-79, doi: 10.1175/2009jcli3071.1, 2010a.

657 Xie, S., McCoy, R. B., Klein, S. A., Cederwall, R. T., Wiscombe, W. J., Jensen, M. P., Johnson,
658 K. L., Clothiaux, E. E., Gaustad, K. L., Long, C. N., Mather, J. H., McFarlane, S. A., Shi, Y.,
659 Golaz, J.-C., Lin, Y., Hall, S. D., McCord, R. A., Palanisamy, G., and Turner, D. D.: CLOUDS
660 AND MORE: ARM Climate Modeling Best Estimate Data, Bulletin of the American
661 Meteorological Society, 91, 13-20, doi: 10.1175/2009BAMS2891.1, 2010b.

662 Yanai, M., Esbensen, S., and Chu, J.-H.: Determination of Bulk Properties of Tropical Cloud
663 Clusters from Large-Scale Heat and Moisture Budgets, Journal of the Atmospheric Sciences, 30,
664 611-627, doi: 10.1175/1520-0469(1973)030<0611:DOBPOT>2.0.CO;2, 1973.

665 Zhang, M., and Lin, J.: Constrained Variational Analysis of Sounding Data Based on Column-
666 Integrated Budgets of Mass, Heat, Moisture, and Momentum: Approach and Application to

667 ARM Measurements, Journal of the Atmospheric Sciences, 54, 1503-1524, doi: 10.1175/1520-
668 0469(1997)054<1503:CVAOSD>2.0.CO;2, 1997.

669 Zhang, M., Lin, J., Cederwall, R. T., Yio, J. J., and Xie, S. C.: Objective Analysis of ARM IOP
670 Data: Method and Sensitivity, Monthly Weather Review, 129, 295-311, doi: 10.1175/1520-
671 0493(2001)129<0295:OAOAID>2.0.CO;2, 2001.

672

Figure and Table Captions:

Table 1: number of convective systems identified in the morning and afternoon during IOP1 and IOP2.

Figure 1: The location of GoAmazon site in this study. The red octagon represents the analysis domain. Locations of observational sites are indicated by yellow pentagrams. Locations of cities are indicated by white dots.

~~Figure 1: The location of GoAmazon site (top) and the analysis domain for this study (bottom). The SIPAM radar is located at Ponta Pelada (indicated by red pentagram). Locations of other cities and measurement sites are also indicated.~~

Figure 2: The sea-level pressure (shaded) and 10-meter horizontal wind (vector) averaged for IOP1 (left) and IOP2 (right). The pentagram indicates the location of GoAmazon site.

Figure 3: Domain averaged time series of (from top to bottom) horizontal (u) wind, meridional (v) wind, relative humidity, cloud frequency (point observation at the ARM site) and precipitation for IOP1 (left) and IOP2 (right). The blank areas in cloud frequency indicate missing data. The three straight black lines in IOP1 show the three cases chosen in section 6.

Figure 4: The time series (top) and temporal mean profiles (bottom) of large-scale vertical velocity for IOP1 (left) and IOP2 (right).

Figure 5: The time series (top) and temporal mean profiles (bottom) of apparent heating source Q_1 for IOP1 (left) and IOP2 (right).

Figure 6: The time series (top) and temporal mean profiles (bottom) of apparent moisture sink Q_2 for IOP1 (left) and IOP2 (right).

Figure 7: The diurnal cycle of precipitation (up) and CAPE and CIN (bottom) for both IOPs.

Figure 8: The diurnal cycle of (from top to bottom) cloud frequency, large-scale vertical velocity, Q_1, Q_2 and $Q_1 - Q_2 - Q_{rad}$ ~~Q_1 Q_2~~ for IOP1 and IOP2. The black lines are zero-lines.

Field Code Changed

Figure 9: SIPAM radar reflectivity snapshots (left) and time series of domain-mean precipitation (right) for three cases of precipitating systems. From top to bottom: LOS, COS and BOS. The black octagons indicate the GoAmazon domain, and the red arrows indicate the propagating direction of the system.

Figure 10: The time series of (a) cloud frequency, (b) relative humidity, (c) surface CAPE and CIN, (d) u wind, (e) v wind, (f) vertical velocity, (g) Q_1, (h) Q_2 and (i) $Q_1 - Q_2 - Q_{rad}$ ~~(a) cloud frequency, (b) surface CAPE and CIN, (c) u wind, (d) v wind, (e) relative humidity, (f) vertical velocity, (g) Q_1 and (h) Q_2~~ for the LOS case. The black lines are zero-lines. The shaded and white areas in (b) indicate nightime and daytime.

Field Code Changed

Figure 11: Similar as Figure 10 but for the COS case.

~~The time series of (a) cloud frequency, (b) surface CAPE and CIN, (c) u wind, (d) v wind, (e) relative humidity, (f) vertical velocity, (g) Q_1 and (h) Q_2 for the COS case. The black lines are zero lines. The shaded and white areas in (b) indicate nighttime and daytime.~~

Figure 12: Similar as Figure 10 but for the BOS case.

~~The time series of (a) cloud frequency, (b) surface CAPE and CIN, (c) u wind, (d) v wind, (e) relative humidity, (f) vertical velocity, (g) Q_1 and (h) Q_2 for the BOS case. The black lines are zero lines. The shaded and white areas in (b) indicate nighttime and daytime.~~

	~~IOP1~~		~~IOP2~~	
	~~Morning~~	~~Afternoon~~	~~Morning~~	~~Afternoon~~
~~Locally Occurring Systems (LOS)~~	~~0~~	~~19~~	~~0~~	~~14~~
~~Coastal Occurring Systems (COS)~~	~~7~~	~~6~~	~~0~~	~~3~~
~~Basin Occurring Systems (BOS)~~	~~3~~	~~3*~~	~~2**~~	~~0~~

~~* the afternoon BOS are continued from the morning time.~~

~~** the two BOS in IOP2 are initialized in the Amazon basin but propagating westward as squall lines.~~

	IOP1		IOP2	
	Morning	Afternoon	Morning	Afternoon
Locally Occurring Systems (LOS)	0	19	0	16
Coastal Occurring Systems (COS)	8	2	0	1
Basin Occurring Systems (BOS)	8	1	3	2

Table 1: number of convective systems identified in the morning and afternoon during IOP1 and IOP2.

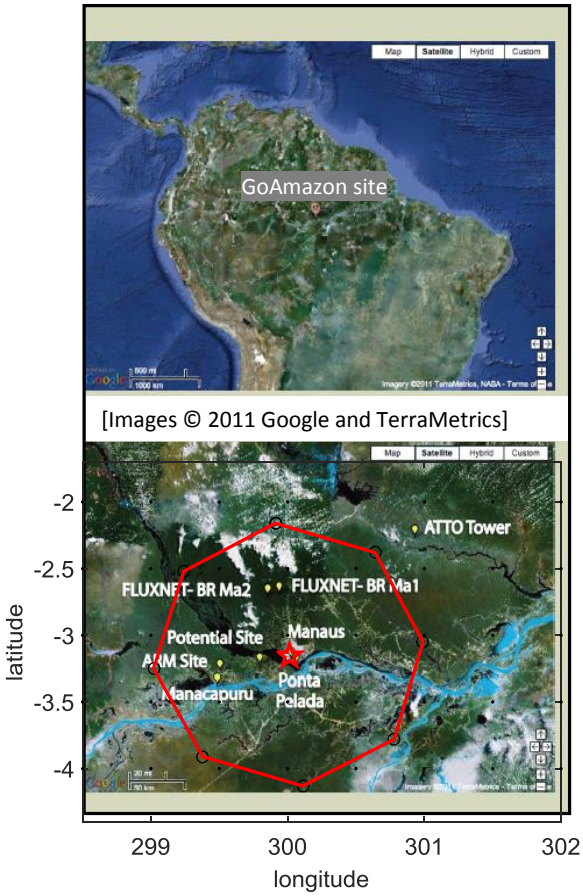

~~Figure 1: The location of GoAmazon site (top) and the analysis domain for this study (bottom). The SIPAM radar is located at Ponta Pelada (indicated by red pentagram). Locations of other cities and measurement sites are also indicated.~~

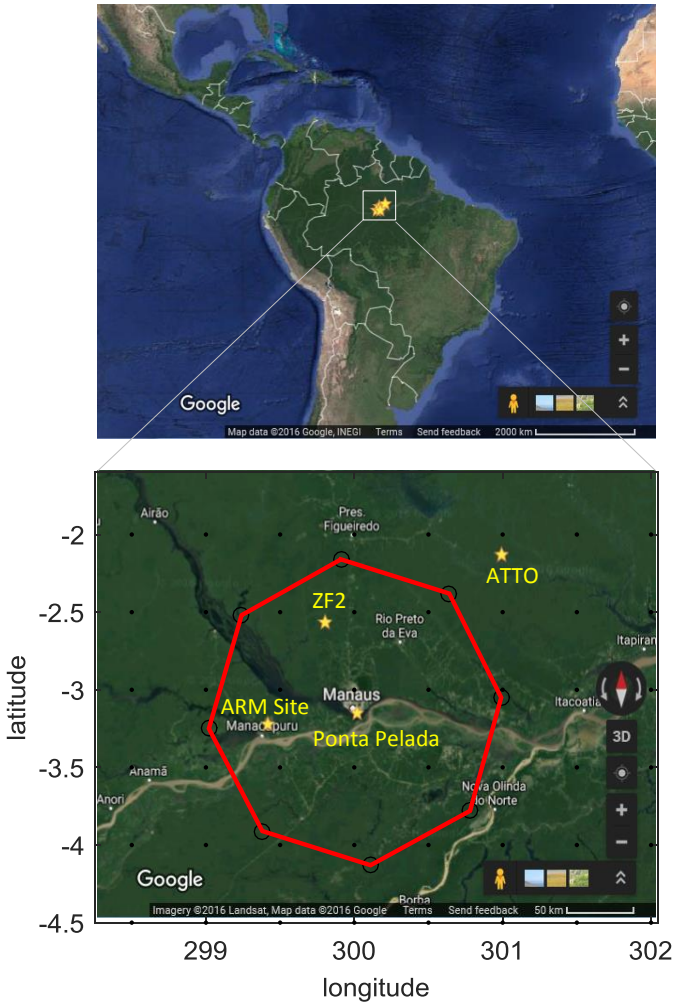

Figure 1: The location of GoAmazon site (top) and the analysis domain for this study (bottom). Locations of measurement sites are indicated by yellow pentagrams. Locations of cities are indicated by white dots.

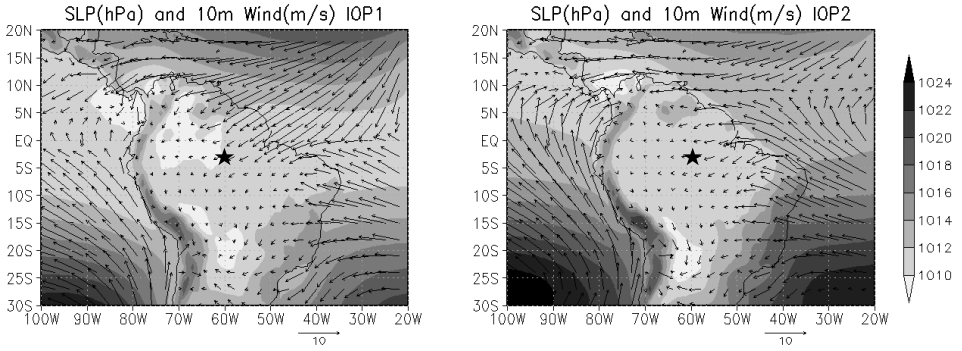

Figure 2: The sea-level pressure (shaded) and 10-meter horizontal wind (vector) averaged for IOP1 (left) and IOP2 (right). The pentagram indicates the location of GoAmazon site.

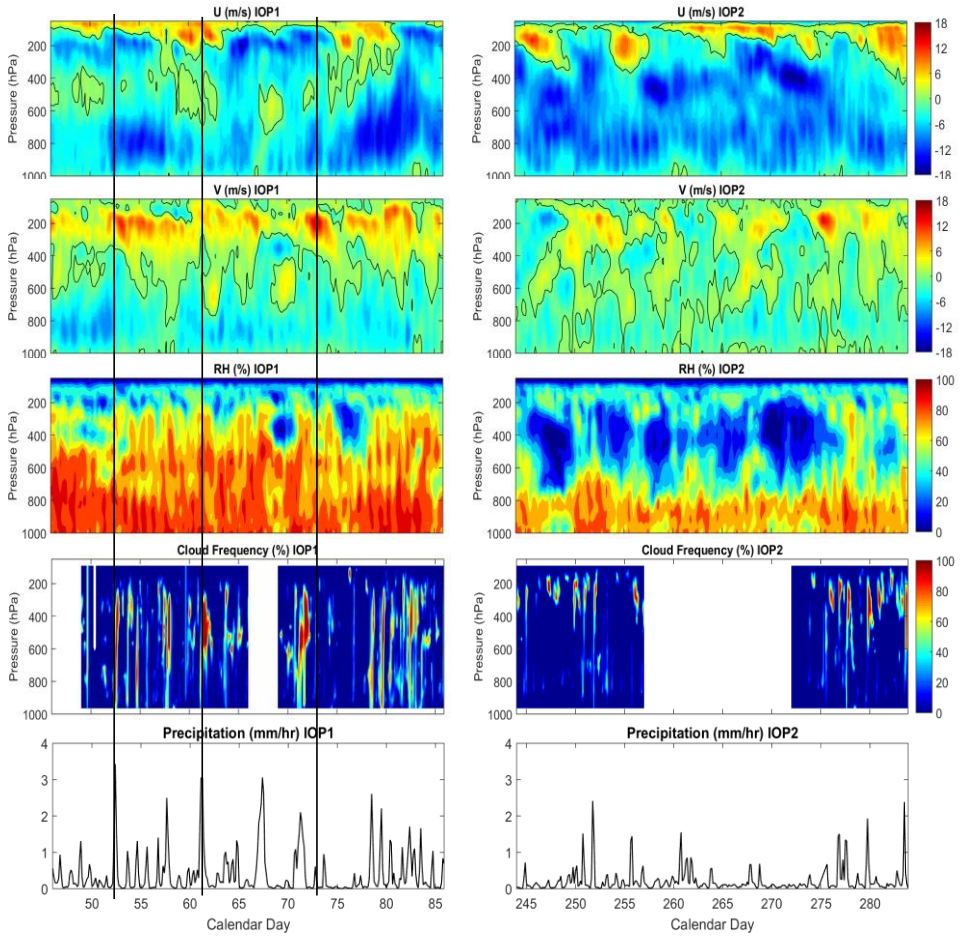

Figure 3: Domain averaged time series of (from top to bottom) horizontal (u) wind, meridional (v) wind, relative humidity, cloud frequency (point observation at the ARM site) and precipitation for IOP1 (left) and IOP2 (right). The blank areas in cloud frequency indicate missing data. The three straight black lines in IOP1 show the three cases chosen in section 6.

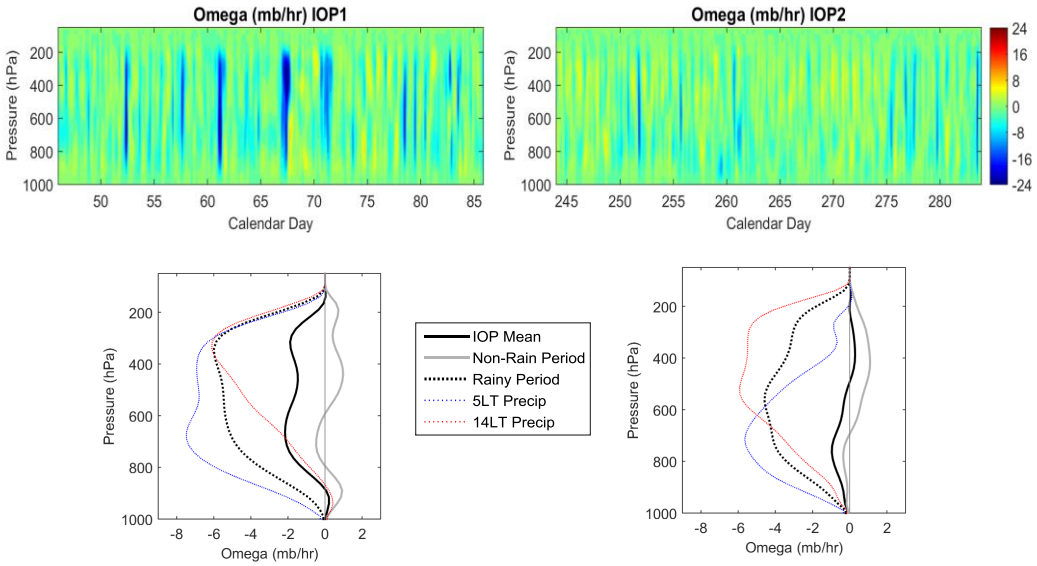

Figure 4: The time series (top) and temporal mean profiles (bottom) of large-scale vertical velocity for IOP1 (left) and IOP2 (right).

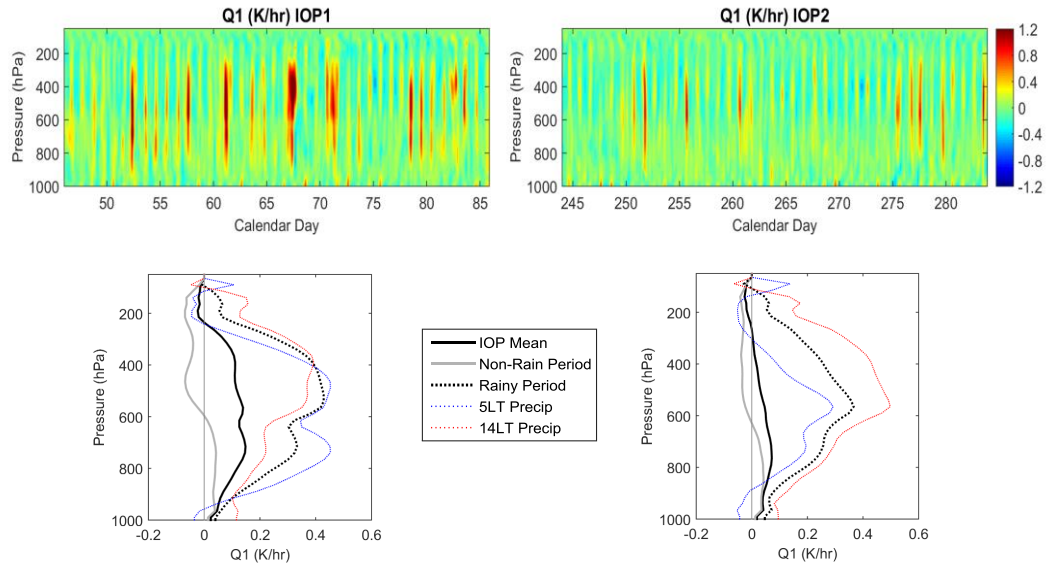

Figure 5: The time series (top) and temporal mean profiles (bottom) of apparent heating source Q_1 for IOP1 (left) and IOP2 (right).

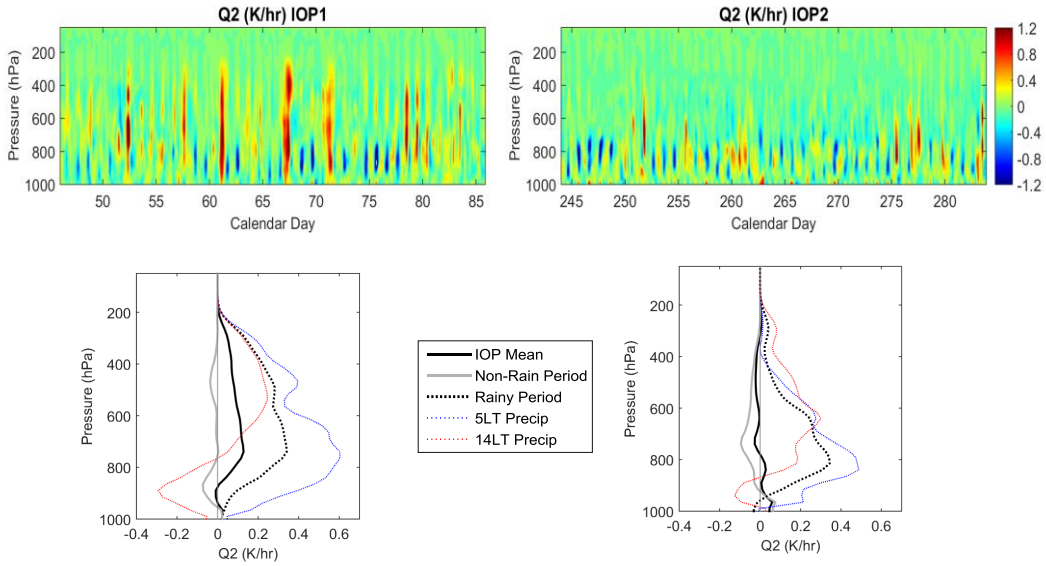

Figure 6: The time series (top) and temporal mean profiles (bottom) of apparent moisture sink Q_2 for IOP1 (left) and IOP2 (right).

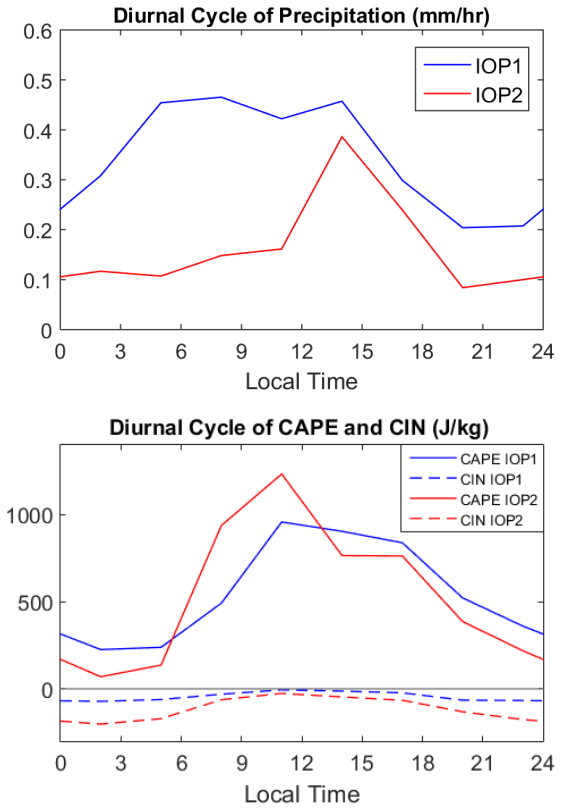

Figure 7: The diurnal cycle of precipitation (up) and CAPE and CIN (bottom) for both IOPs.

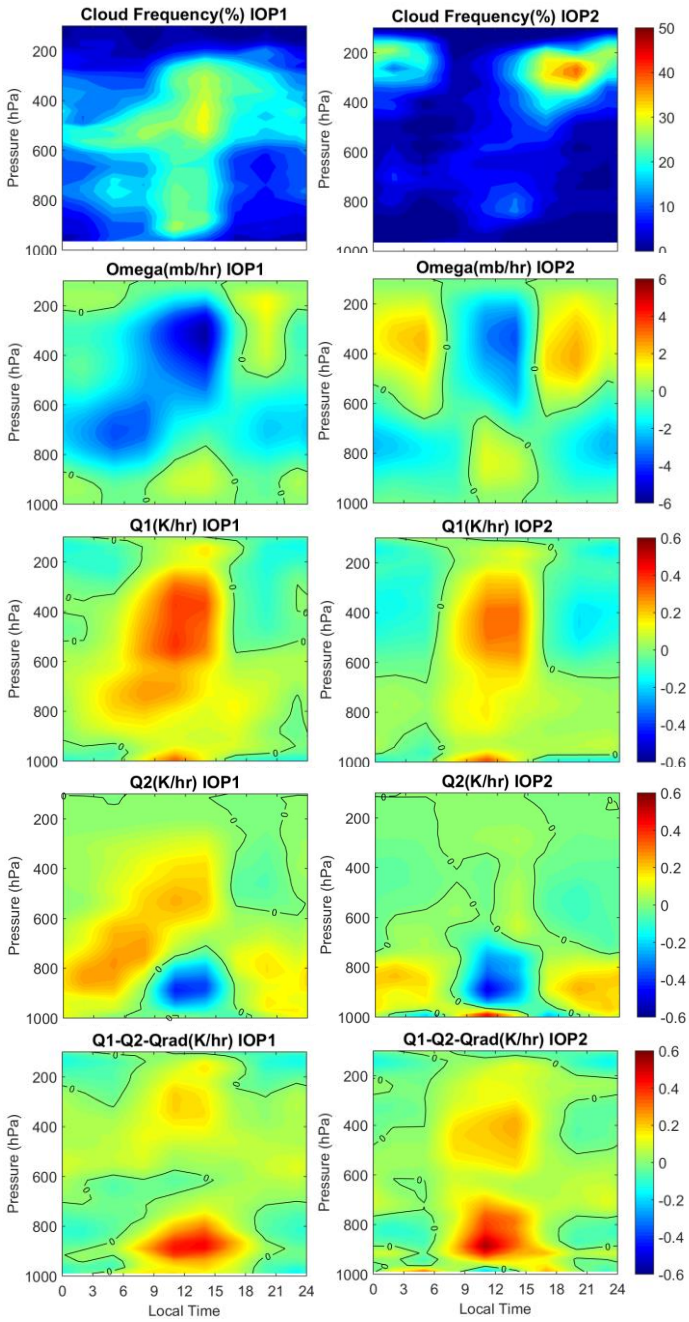

Figure 8: The diurnal cycle of (from top to bottom) cloud frequency, large-scale vertical velocity, Q_1, Q_2 and $Q_1 - Q_2 - Q_{rad}$ for IOP1 and IOP2. The black lines are zero-lines.

Field Code Changed

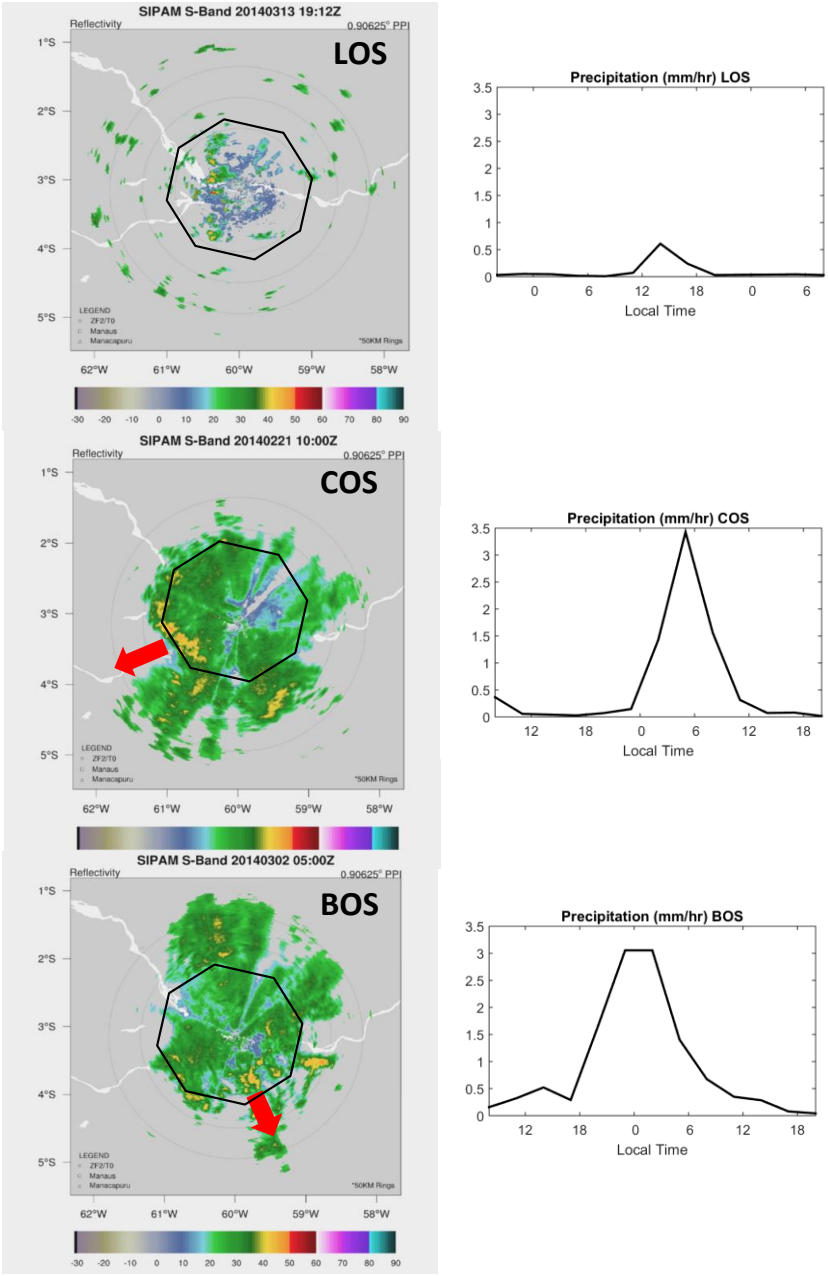

819

820 Figure 9: SIPAM radar reflectivity snapshots (left) and time series of domain-mean precipitation (right)
821 for three cases of precipitating systems. From top to bottom: LOS, COS and BOS. The black octagons
822 indicate the GoAmazon domain, and the red arrows indicate the propagating direction of the system.

823

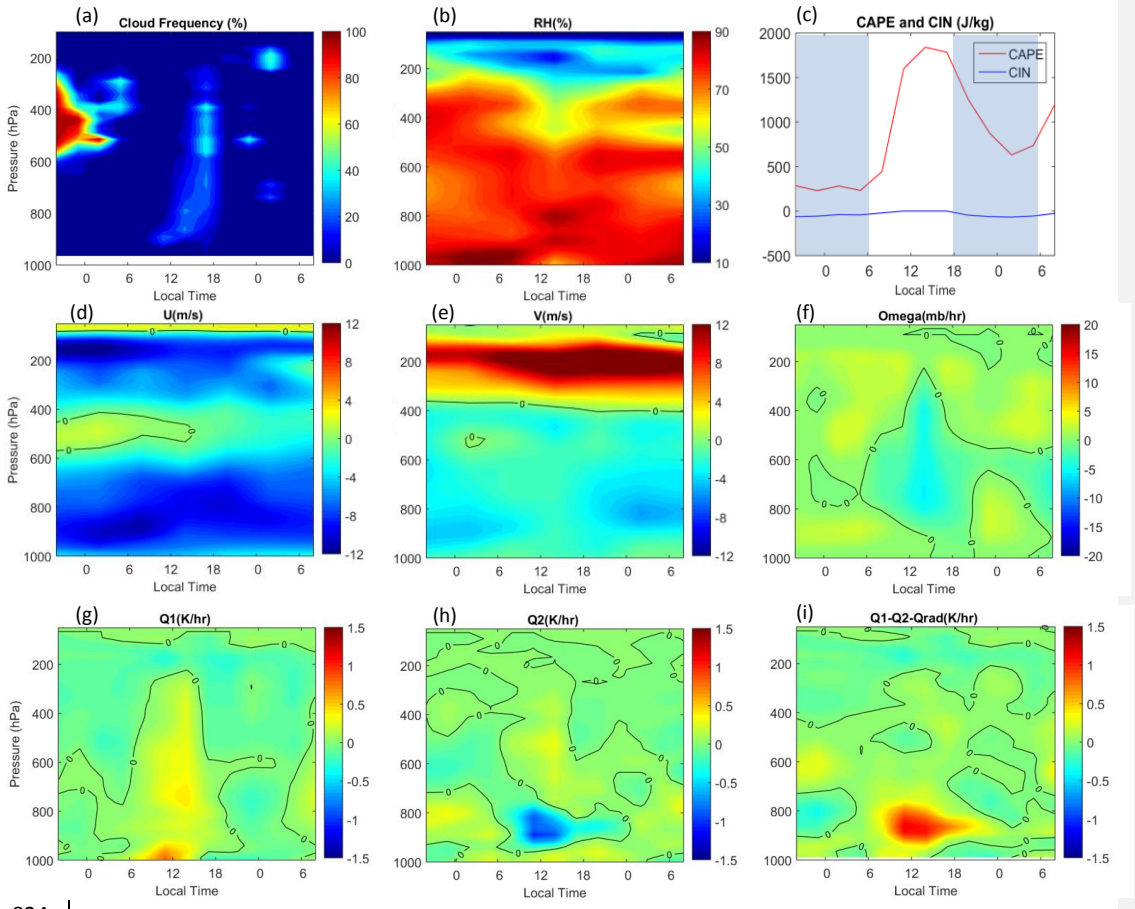

Figure 10: The time series of (a) cloud frequency, (b) relative humidity, (c) surface CAPE and CIN, (d) u wind, (e) v wind, (f) vertical velocity, (g) Q_1, (h) Q_2 and (i) $Q_1 - Q_2 - Q_{rad}$ for the LOS case. The black lines are zero-lines. The shaded and white areas in (c) indicate nighttime and daytime.

Field Code Changed

829

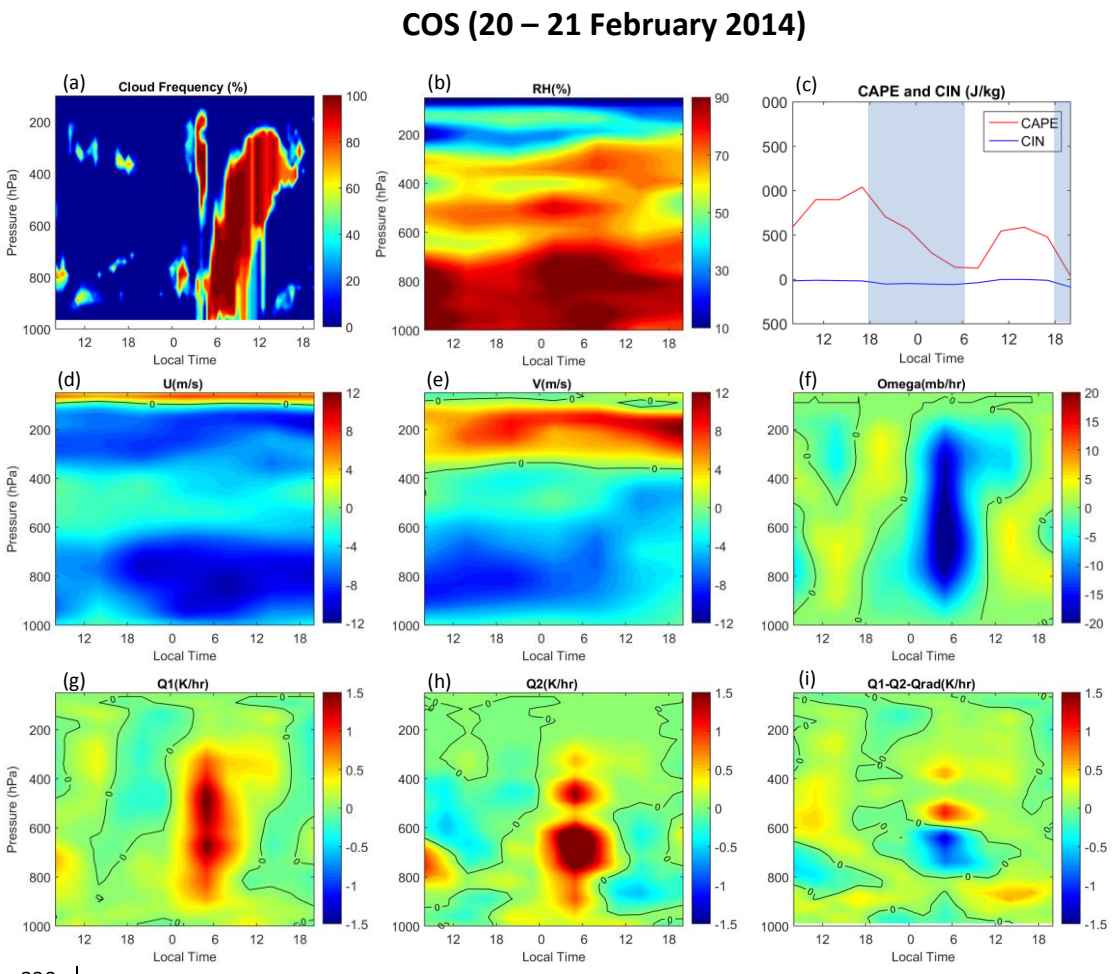

830

831 Figure 11: Similar as Figure 10 but for the COS case.

832

833

834

835

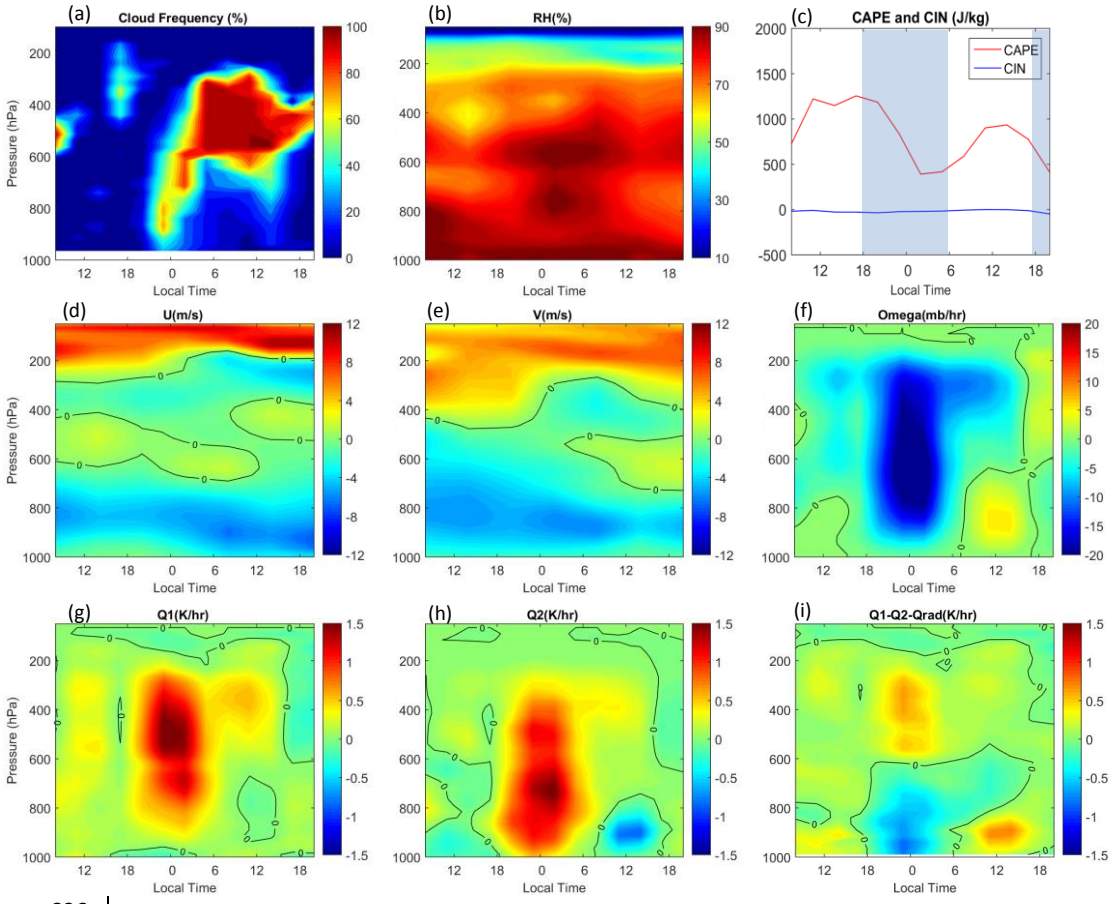

Figure 12: Similar as Figure 10 but for the BOS case.

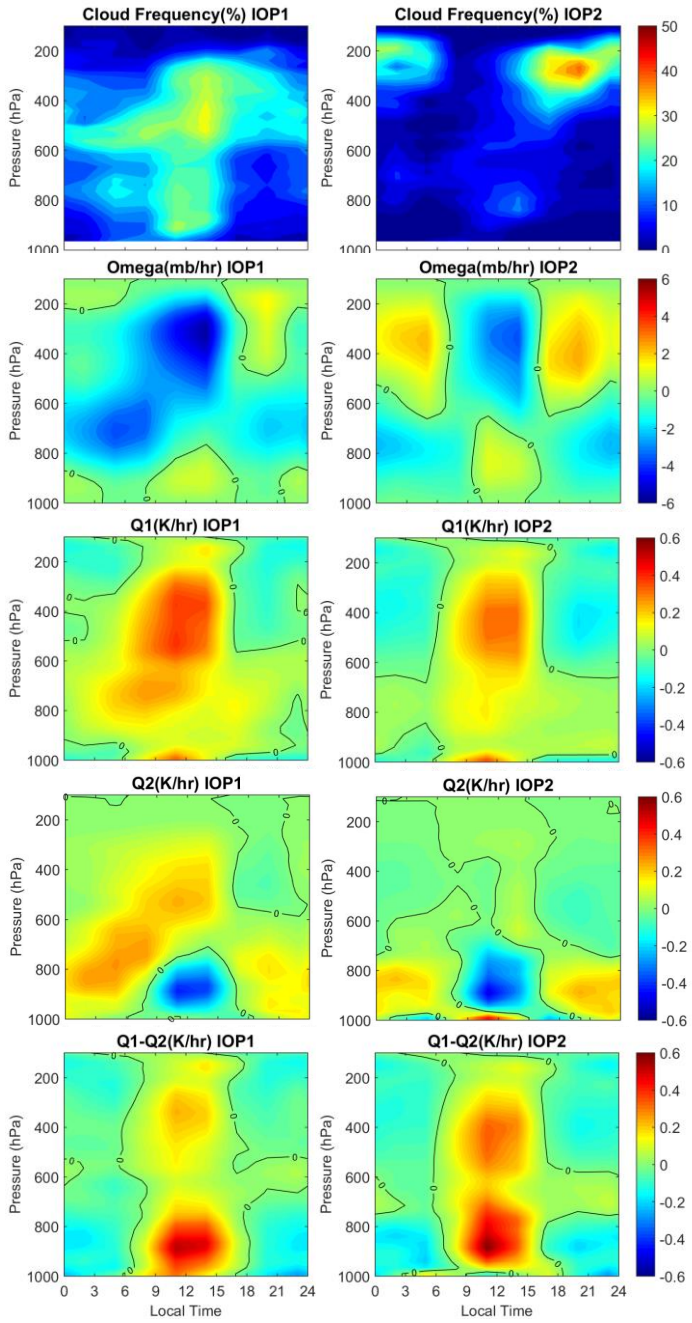
Cloud Frequency(%) IOP1
Cloud Frequency(%) IOP2
Omega(mb/hr) IOP1
Omega(mb/hr) IOP2
Q1(K/hr) IOP1
Q1(K/hr) IOP2
Q2(K/hr) IOP1
Q2(K/hr) IOP2
Q1-Q2(K/hr) IOP1
Q1-Q2(K/hr) IOP2
Pressure (hPa)
Local Time

839

~~Figure 8: The diurnal cycle of (from top to bottom) cloud frequency, large-scale vertical velocity, Q_1, Q_2 and Q_1 – Q_2 for IOP1 and IOP2. The black lines are zero-lines.~~

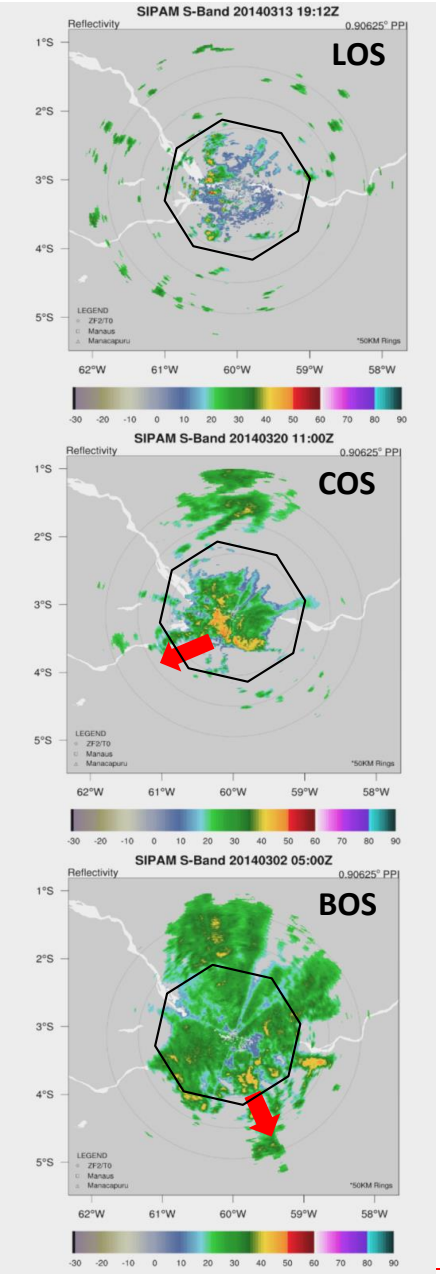

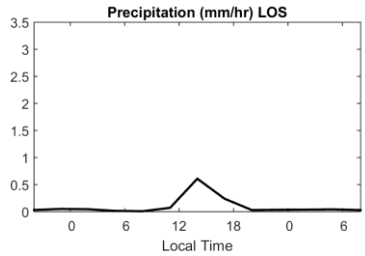

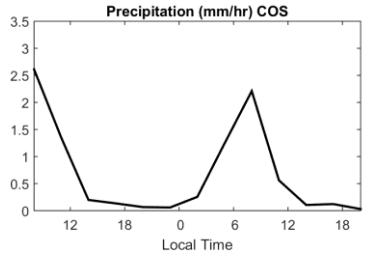

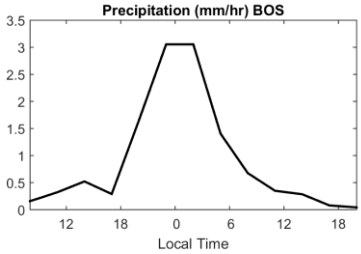

843 ~~Figure 9: SIPAM radar reflectivity snapshots (left) and time series of domain-mean precipitation (right)~~
844 ~~for three cases of precipitating systems. From top to bottom: LOS, COS and BOS. The black octagons~~
845 ~~indicate the GoAmazon domain, and the red arrows indicate the propagating direction of the system.~~

846

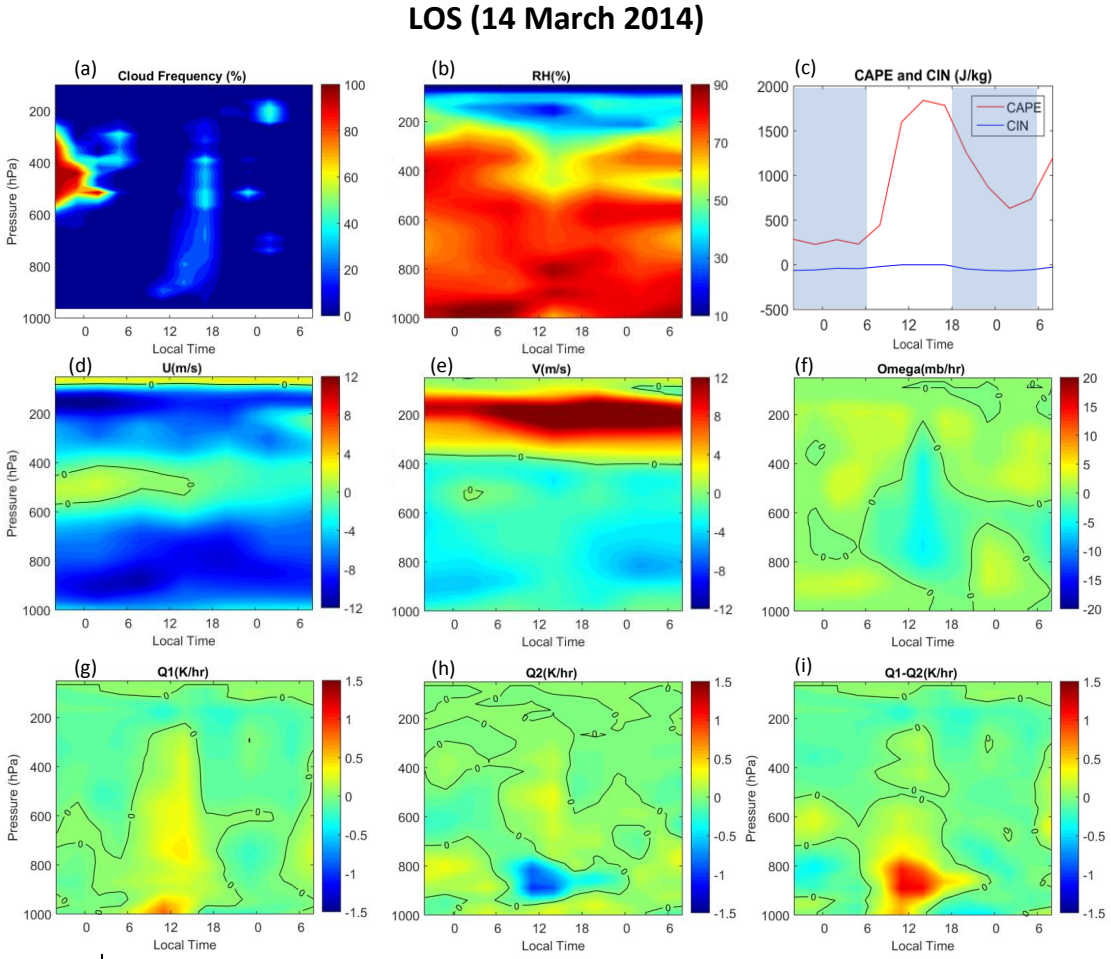

847

848 ~~Figure 10: The time series of (a) cloud frequency, (b) relative humidity, (c) surface CAPE and CIN, (d) u~~
849 ~~wind, (e) v wind, (f) vertical velocity, (g) Q_1, (h) Q_2 and (i) $Q_1 - Q_2$ for the LOS case. The black lines are~~
850 ~~zero-lines. The shaded and white areas in (c) indicate nighttime and daytime.~~

851

852

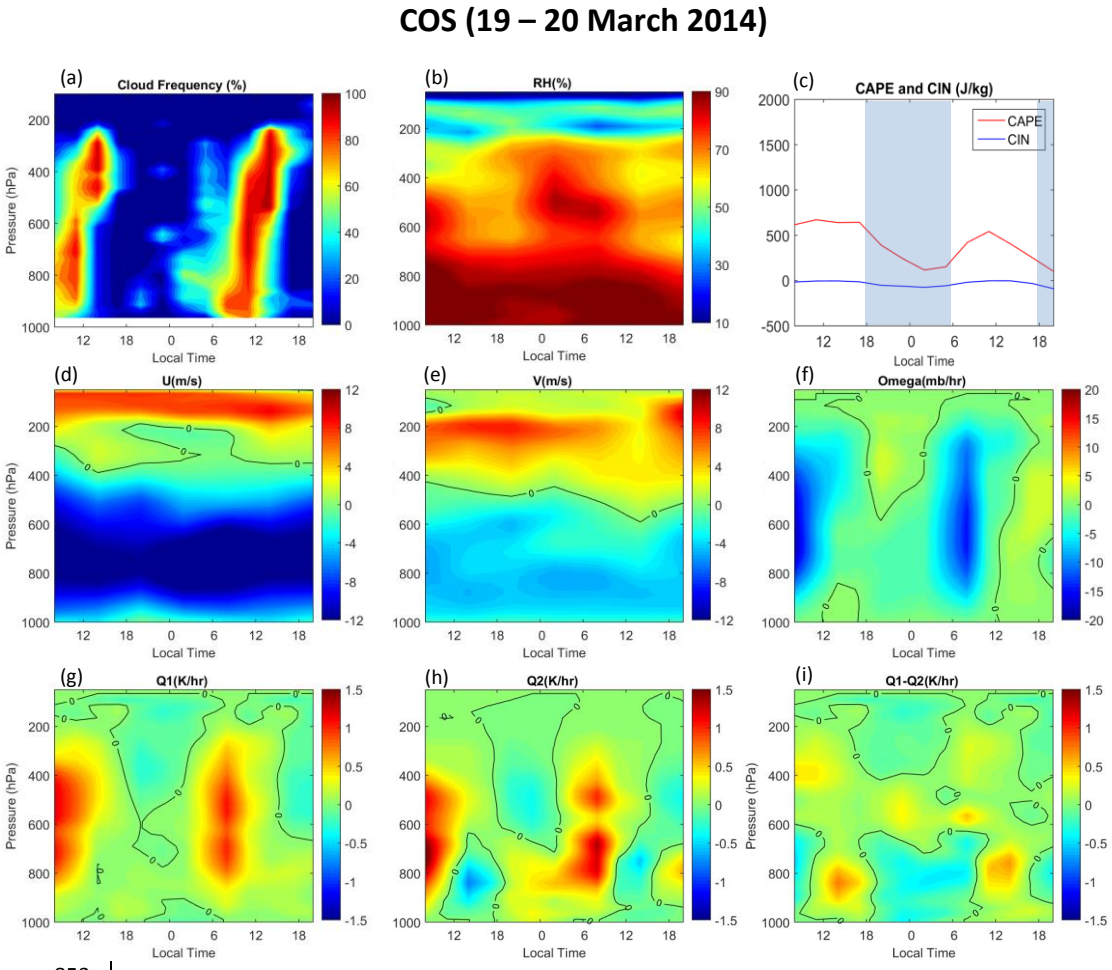

853

854 ~~Figure 11: Similar as Figure 10 but for the COS case.~~

855

856

857

858

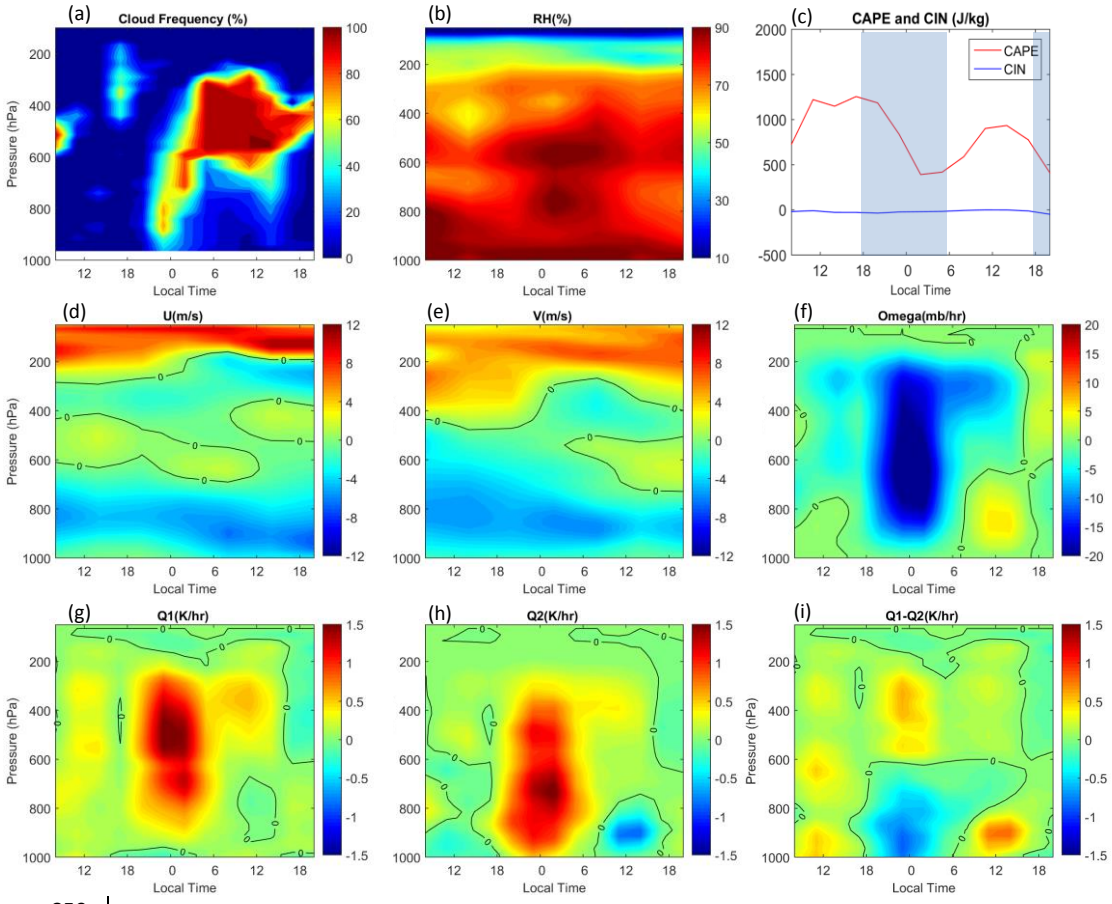

859

860 ~~Figure 12: Similar as Figure 10 but for the BOS case.~~